Fluorescent- and tagged-protoxin II peptides: potent markers of the Na v 1.7 channel pain target

Jérôme Montnach, Stephan de Waard, Sébastien Nicolas, Sophie Burel, Nancy Osorio, Claude Zoukimian, Massimo Mantegazza, Rachid Boukaiba, Rémy Béroud, Michel Partiseti, et al.

RESEARH PAPER

Title: Fluorescent- and tagged-protoxin II peptides: potent markers of the $Na_v1.7$ channel pain target

Running Title: Investigation of the $Na_v1.7$ channel with new protoxin II analogues

Full names of the authors: Jérôme Montnach[§], Stephan De Waard[§], Sébastien Nicolas[§], Sophie Burel[§], Nancy Osorio[¶], Claude Zoukimian[‡], Massimo Mantegazza[‡], Rachid Boukaiba[†], Rémy Béroud[‡], Michel Partiseti[†], Patrick Delmas[¶], Céline Marionneau[§], Michel De Waard[§,§,*]

Author's institutional affiliations: [§] l'institut du thorax, INSERM, CNRS, UNIV NANTES, LabEx "Ion Channels, Science & Therapeutics", F-44007 Nantes, France. [¶] Laboratory of Cognitive Neuroscience, UMR 7291, CNRS, Aix-Marseille University, F-13015 Marseille Cedex 15, France. [‡] Smartox Biotechnology, 6 rue des Platanes, F-38120 Saint-Egrève, France. [‡] Université Cote d'Azur, CNRS UMR 7275, Institute of Molecular and Cellular Pharmacology, Valbonne-Sophia Antipolis, France. [†] Sanofi R&D, Integrated Drug Discovery – High Content Biology, F-94440 Vitry-sur-Seine, France.

*** Corresponding author:** Michel De Waard, l'institut du thorax, INSERM, CNRS, UNIV NANTES, LabEx "Ion Channels, Science & Therapeutics", F-44007 Nantes, France. Phone: +33 228 080 076 – E-mail: michel.dewaard@univ-nantes.fr or dewaard@smartox-biotech.com - ORCID 0000-0002-2782-9615.

Data availability statement: The data that support the findings of this study are available from the corresponding author upon reasonable request. Some data may not be made available because of privacy or ethical restrictions.

Word counts (excluding abstract, methods, references and figure legends): **Introduction** 928 + **Results** 5222 + **Discussion** 1210 = 7360.

Acknowledgements: M. De Waard thanks the Agence Nationale de la Recherche for its financial support to the laboratory of excellence "Ion Channels, Science and Therapeutics" (grant N° ANR-11-LABX-0015). This work was supported by the Fondation Leducq in the frame of its program of ERPT equipment support (purchase of an automated patch-clamp system), by a grant "New Team" of the Région Pays de la Loire to M. De Waard, and by a European FEDER grant in support of the automated patch-clamp system of Nanion. The salary of S. Nicolas is supported by the Fondation Leducq, while the fellowship of J. Montnach is provided by a National Research Agency Grant to M. De Waard entitled Bradycardia (grant N° ANR-15-CE14-0004-02). We thank the PicroPicell platform also for invaluable help with confocal imaging.

Conflict of interest statement: The authors C. Zoukimian and R. Béroud declare the following competing interest: current employees of Smartox, while R. Boukaiba and M. Partiseti declare being current employees of Sanofi.

Author contributions: S.N., S.D.W., S.B, N.O., P.D., M.M., C.M. and J.M. performed cell culture, automated patch-clamp, biochemistry and histochemistry experiments and analyses. C.Z. and R. Béroud performed the chemical syntheses of ProTx II analogues and other peptides. R. Boukaiba and M.P. performed selectivity experiments with various Na_v channel isoforms. J.M. and M.D.W. made the figures. M.D.W. managed the project and wrote the manuscript.

What is already known

- ProTx-II, a lead peptide for pain treatment, blocks hNa_v1.7 channel with high affinity.

What this study adds

- New functionalized ProTx-II analogues can be chemically produced that best preserve the native peptide activity.
- The new tagged analogues have valuable properties for biochemistry and distribution studies of Na_v1.7 channel.

Clinical significance

- These ProTx-II analogues enrich the molecular arsenal required for Na_v1.7 studies and drug screening campaigns.

ABSTRACT

BACKGROUND AND PURPOSE

Protoxin II (ProTx II) is a high affinity gating modifier that is thought to selectively block the $Na_v1.7$ voltage-dependent Na^+ channel, a major therapeutic target for the control of pain. We aimed at producing ProTx II analogues entitled with novel functionalities for cell distribution studies and biochemical characterization of its Na_v channel targets.

EXPERIMENTAL APPROACH

We took advantage of the high affinity properties of the peptide, combined to its slow off rate, to design a number of new tagged analogues useful for imaging and biochemistry purposes. We used high-throughput automated patch-clamp to identify the analogues best matching the native properties of ProTx II and validated them on various Na_v-expressing cells in pull-down and cell distribution studies.

KEY RESULTS

Two of the produced ProTx II analogues, Biot-ProTx II and ATTO488-ProTx II, best recapitulate the pharmacological properties of unlabelled ProTx II, while other analogues remain high affinity blockers of $Na_v1.7$. The biotinylated version of ProTx II efficiently works for the pull-down of several Na_v isoforms tested in a concentration-dependent manner, while the fluorescent ATTO488-ProTx II specifically labels the $Na_v1.7$ channel over other Na_v isoforms tested in various experimental conditions.

CONCLUSIONS AND IMPLICATIONS

The properties of these ProTx II analogues as tools for Na_v channel purification and cell distribution studies pave the way for a better understanding of ProTx II channel receptors in pain and their pathophysiological implications in sensory neuronal processing. The new fluorescent ProTx II should also reveal itself useful for the design of new drug screening strategies.

Key Words: Protoxin II, $Na_v1.7$, voltage-gated sodium channel, pain target, automated patch-clamp, fluorescent analogue, biotinylated analogue, cell line, cellular distribution, pull-down.

Abbreviations: CHO, Chinese Hamster Ovary; ProTx II, Protoxin II; HEPES, N-2-hydroxyethylpiperazine-N'-2-ethanesulfonic acid; IC_{50}, peptide concentration required to inhibit 50% of the response; Na_v, voltage-gated sodium channel.

1 INTRODUCTION

Contribution of $Na_v1.7$ to pain sensation - Voltage-gated sodium channels (Na_v) contribute to cell excitability by elaborating and propagating action potentials. Several genetic reports in mice and humans highlight the role played by $Na_v1.7$ in pain. In humans, missense mutations of the *SCN9A* gene result in Congenital Indifference to Pain (CIP, (Cox et al., 2006)). A similar phenotype is observed in the *Scn9a* knockout mouse (Gingras et al., 2014; Nassar et al., 2004). Several other pain syndromes have been associated to $Na_v1.7$ mutations: (i) paroxysmal extreme pain disorder (PEPD) for mutations impairing fast channel inactivation and promoting persistent current (Fertleman et al., 2006), (ii) painful small fibre neuropathy (Hoeijmakers et al., 2012), (iii) idiopathic small fibre neuropathy by mutations affecting fast and slow inactivation (Faber et al., 2012), and (iv) primary erythromelalgia for mutations that lower $Na_v1.7$ threshold of activation (Cummins, Dib-Hajj & Waxman, 2004; Dib-Hajj et al., 2005; Fischer & Waxman, 2010).

Initiatives to develop potent $Na_v1.7$ blockers - These observations all motivated the development of $Na_v1.7$-selective blockers for pain treatment. Since human patients that lack $Na_v1.7$ channel activity, experience solely anosmia (Weiss et al., 2011), in addition to CIP, potent $Na_v1.7$ channel blockers should have limited side effects (Cox et al., 2006). The level of sequence homologies among Na_v isoforms being high, the search for selective compounds is a real challenge. Drugs that have been among the most successful in reaching high selectivity levels among sodium channels are animal toxins of peptide origin. Two reasons explain this success: firstly, toxins bind onto the channel through multiple interactions thanks to larger chemical spaces, and secondly, most toxins are gating modifiers and bind onto voltage sensor domains that are less conserved in sequence. Therefore, toxin binding sites represent interesting lead hot spots for the development of new organic drugs that have better oral bioavailability profiles. Spider venoms have been proficient in providing lead compounds active on $Na_v1.7$ (Nicolas et al., 2019).

The particular case of Protoxin II - Protoxin II (ProTx II), from the venom of the tarantula spider *Thrixopelma pruriens*, is one of the most selective and potent peptides active on $Na_v1.7$ (Middleton et al., 2002; Smith, Cummins, Alphy & Blumenthal, 2007), although a full pharmacological profiling is lacking, namely with regard to ProTx II activity on $Na_v1.9$. ProTx II is a 30-mer three disulphide-bridged peptide which folds according to the classical inhibitor cysteine knot (ICK) motif (Cys^1-Cys^4, Cys^2-Cys^5 and Cys^3-Cys^6 pattern) and hence belongs to the NaSpTx3 family. It inhibits $Na_v1.7$ currents at concentrations close to 1 nM (Schmalhofer

et al., 2008), mainly by trapping the voltage-sensor. The IC_{50} values on other $Na_v1.x$ isoforms is incidentally higher (between 30 and 150 nM). For $Na_v1.5$, the block can be reversed by strong depolarisations suggesting that binding affinity may vary as a function of channel state (Sokolov, Kraus, Scheuer & Catterall, 2008). The C-terminal tail of ProTx II is a major determinant of the potency and selectivity of the toxin on $Na_v1.7$ (Park et al., 2014). A chimera channel, made of the bacterial Na_v and the domain II voltage sensor S1-S4 of $Na_v1.7$, recapitulates ProTx II block (Rajamani et al., 2017). The complete structural basis of $Na_v1.7$ channel inhibition by ProTx II was revealed by Cryo-EM studies (Xu et al., 2019). The block of the channel requires several priming steps: (i) a proper membrane partitioning to enhance local ProTx II concentration in the vicinity of $Na_v1.7$ thanks to an aromatic-rich surface (comprising W5, W7, W24 and W30), and (ii) a lipid environment-imposed positioning of the toxin combined to a two-dimensional restricted binding site search. Binding of ProTx II involves the $Na_v1.7$ LFLAD motif present in the domain II S3-S4 loop and uses W24 as a hydrophobic anchor for engaging binding and the two basic charge chains of R22 and K26 to target E811, D816 and eventually E818 depending on the channel state (activated *versus* deactivated). The mechanism of action of current inhibition implies an electrostatic modulation of the voltage sensor. The therapeutic efficacy of ProTx II remains conflicting. ProTx II has little efficacy on short-term or inflammatory pain probably because it does not cross the blood-nerve barrier (Lim et al., 2014; Schmalhofer et al., 2008). However, intrathecal injection of ProTx II neutralizes persistent post-surgical pain (Li et al., 2017) and counteracts hyperalgesia in diabetic mice (Tanaka, Sekino, Ikegami, Ikeda & Kamei, 2015). Finally, intraperitoneal injection reduces burn injury-induced spinal nociceptive processing (Torres-Perez, Adamek, Palecek, Vizcaychipi, Nagy & Varga, 2018).

Using ProTx II as a molecular tool to characterize $Na_v1.7$ further – Despite the therapeutic importance of $Na_v1.7$, appropriate molecular tools to investigate its functional properties or to facilitate drug discovery process are still lacking. The quality of $Na_v1.7$ remain questionable (Lee et al., 2014; Liu et al., 2016). We decided to capitalize on the knowledge accumulated on ProTx II SAR to develop ProTx II-derived tools that would facilitate the investigation of $Na_v1.7$ channel function, biochemistry and distribution in neuronal tissues or the search for novel analgesics. We herein present the chemical syntheses and characterization of several new ProTx II analogues that bind with high affinity onto $Na_v1.7$ and preserve a good selectivity for this channel type over other channels: a biotinylated version, a poly-his-tagged and two new fluorescent ProTx II analogues. The best fluorescent analogue allows labelling of $Na_v1.7$ channels in re-expression system by cell cytometry or in confocal imaging experiments, while

the biotinylated version of ProTx II authorizes $Na_v1.7$ channel pull-down and biochemical investigations. These new optimized tools should facilitate the understanding of ProTx II-sensitive Na_v channel contribution to pain and their pathophysiological implications in sensory neuronal processing.

2 METHODS

2.1 Chemical syntheses of ProTx II / ProTx II K26E and fluorescent analogues

ProTx II and ProTx II K26E were assembled stepwise using a 2-chlorotrityl chloride resin (initial substitution rate of 1.6 mmol/g) by solid-phase fmoc chemistry on a Symphony Synthesizer (Protein technologies Inc., Tucson, USA). The coupling reaction of each amino acid with HCTU and collidine took 15 min and the reaction is repeated three times to increase the amino acid coupling yield. Pentynoic acid was coupled at the end of the synthesis for the fluorescent analogues. After resin cleavage and deprotection with TFA / iPr_3SiH / 1,3-dimethoxybenzene / 2,2′-(ethylenedioxy)diethanethiol / H_2O (85:2.5:3.75:3.75:5), the peptides were folded in an oxidative buffer containing oxidized and reduced gluthatione and purified to homogeneity by C18 RP-HPLC on a Jupiter Proteo column (Phenomenex, 4 µm, 21.2 mm ID x 250 mm L) using an Agilent Technologies preparative HPLC (1260 Infinity). Fluorescent probes were added by click chemistry using 5 equivalents of ATTO488 azide or Cy5 azide, 10 equivalents of CuBrDMS and 50 equivalents of THPTA. After 5 hrs, the mixture was purified to homogeneity by C18 RP-HPLC on a Jupiter Proteo column (Phenomenex, 4 µm, 21.2 mm ID x 250 mm L) using an Agilent Technologies preparative HPLC (1260 Infinity). The molecular masses of ProTx II / ProTx II K26E and fluorescent analogues were determined by LC-ESI-QTOF MS.

2.2 Cell cultures

2.2.1 CHO and HEK293 cells - CHO cells stably expressing the human (h) $Na_v1.7$ channel were cultured in Dulbecco's Modified Eagle's Medium (DMEM) supplemented with 10% foetal calf serum, 1 mM pyruvic acid, 4 mM glutamine, 10 U/mL penicillin and 10 µg/mL streptomycin (Gibco, Grand Island, NY), and incubated at 37°C in a 5% CO_2 atmosphere. For electrophysiological recordings, cells were detached with trypsin and floating single cells were diluted (~300,000 cells/mL) in medium contained (in mM): 4 KCl, 140 NaCl, 5 glucose, 10 HEPES (pH 7.4, osmolarity 290 mOsm). Similar culturing conditions were used for CHO cells transiently expressing $hNa_v1.4$ and stable HEK293 cell lines expressing $hNa_v1.1$, $hNa_v1.2$, $hNa_v1.3$, $hNa_v1.5$ and $hNa_v1.6$ channels. The plasmid $h\beta_3$-IRES-YFP (Rusconi et al., 2007) was

used for transient expression in CHO-hNa_v1.7 cells using the Maxcyte electroporation system.

2.2.2 DRG neurons - Dissociation of DRG neurons has been previously described (Coste, Crest & Delmas, 2007). In brief, cultures of DRG neurons were established from young male C57BL/6 mice. Mice are placed in a chamber perfused with 4% isoflurane for anaesthesia and then decapitated. Excised DRG ganglia were incubated in enzyme solution containing 2 mg/mL of collagenase IA (Invitrogen) for 45 min at 37°C and triturated in Hanks' medium (Invitrogen). Once dissociated, cells were plated on 12-mm coverslips precoated with laminin and poly-D-lysine (Bioboat, Corning) and allowed to attach for 2 min before adding culture medium consisting of DMEM supplemented with 10% heat-inactivated foetal calf serum, 50 U/mL penicillin-streptomycin, 25 mM glucose, 2 mM L-glutamine, 25 ng/mL nerve growth factor, and 4 ng/mL glial-derived neurotrophic factor (all from Invitrogen). Cells were maintained in a humidified atmosphere (5% CO_2, 37°C) for 24-96 hrs before staining.

2.2.3 Cerebellar granule cells - Cerebellar granule neurons have been isolated from 7 days-old mice as previously described (Bilimoria & Bonni, 2008). Briefly, after isolation of cerebella and mechanical dissociation of cells, the cell pellet was washed three times in HHGN solution (Sigma) and cells plated onto poly-lysine coated coverslips in culture medium (DMEM, 10% foetal bovine serum, 4 mM glutamine, 10 U/mL penicillin and 10 µg/mL streptomycin (Gibco, Grand Island, NY)), and incubated at 37°C in a 5% CO_2 atmosphere. KCl (25 mM, Sigma) has been added to the cell culture 24 hr after plating.

2.3 Automated patch-clamp recordings and pharmacological studies

Whole–cell recordings were used to investigate the effects of the toxins on CHO or HEK293 cells expressing the various hNa_v1.7 channels. Automated patch-clamp recordings were performed using the SyncroPatch 384PE from Nanion (München, Germany). Chips with single-hole medium resistance of 5.14 ± 0.02 MΩ (n=384) were used for CHO or HEK293 cell recordings. Pulse generation and data collection were performed with the PatchControl384 v1.5.2 software (Nanion) and the Biomek v1.0 interface (Beckman Coulter). Whole-cell recordings were conducted according to the recommended procedures of Nanion. Cells were stored in a cell hotel reservoir at 10°C with shaking speed at 60 RPM. After initiating the experiment, cell catch, sealing, whole-cell formation, liquid application, recording, and data acquisition were all performed sequentially and automatically. The intracellular solution contained (in mM): 10 CsCl, 110 CsF, 10 NaCl, 10 EGTA and 10 HEPES (pH 7.2, osmolarity

280 mOsm), and the extracellular solution contained (in mM): 100 NaCl, 4 KCl, 40 NMDG, 2 $CaCl_2$, 1 $MgCl_2$, 5 Glucose and 10 HEPES (pH 7.4, osmolarity 298 mOsm). Whole-cell experiments were performed at a holding potential of −100 mV at room temperature (18-22°C). Currents were sampled at 20 kHz. Each peptide was prepared at various concentrations in the extracellular solution, itself supplemented with 0.3% bovine serum albumin. The peptides were distributed in 384-well compound plates according to the number of peptides to be tested, the concentration to be tested, and the number of cells desired for each experimental condition. This distribution within compound plates could not be randomized since it subsequently would excessively complexify the methods of analyses. A single toxin concentration was applied to each cell and a minimum of n=16 cells were recorded for a given peptide concentration. All dose-response curves were built using 7 concentrations and therefore a minimum of a total of n=16x7= 112 cells for each peptide. With such a high n value for doses-responses, we did not perform prospective power analysis. Also, triplicates were never used. The working compound solution was diluted 3 times in the patch-clamp recording well by adding 30 to 60 µL external solution to reach the final reported concentration and the test volume of 90 µL. For establishing dose-response curves, the compounds were tested at a test potential of 0 or 10 mV (depending on channel activation properties) with a pulse every 5 sec. The percentage of current inhibition by the peptides was measured at equilibrium of blockage or at the end of a 14-min application time. Activation curves were built by 50 ms-lasting depolarisations from -70 mV to 70 mV using 5 mV increment steps. Pulses were applied every 5 sec. Steady-state inactivation curves were conducted by varying a 1-sec prepulse potential from -120 mV to 0 mV according to 5 mV incremental steps and using a 50 ms-lasting depolarization step to 0 mV. Pulses were applied every 10 sec, time during which cells were mostly hold at -100 mV before prepulse and pulse application. Activation and steady-state inactivation were performed in both control conditions and in conditions of peptide-induced partial $Na_v1.7$ current block (40 to 60%).

2.4 Cell fluorescence quantification experiments

The specificity of ATTO488-ProTx II was evaluated with a fluorescence-activated cell sorting (FACS) (BD Biosciences). CHO and CHO-h$Na_v1.7$ cells were seeded onto Petri dishes in complete medium and grown to 80% confluence. Cells were treated with trypsin, washed, resuspended in a solution contained 140 NaCl, 4 KCl, 5 glucose and 10 HEPES (pH 7.4, osmolarity 290 mOsm), and 0.5 millions of cells (1 million/mL) were incubated for 20 min with 300 nM or 1 µM ATTO488-ProTx II at room temperature. To check the binding specificity, some cells were preincubated with 10 µM of ProTx II during 20 min prior ATTO488-ProTx II

incubation (2 μM). After washing and gating on live (gate 1, **Supplementary Figure 12**) and single cells (gate 2, **Supplementary Figure 12**), bound ATTO488-ProTx II molecules were detected. Data were analysed using FCS Express 6 software (DeNovo software).

2.5 Cell staining with ATTO488-ProTx II / ATTO488-ProTx II K26E and Cy5-ProTx II and confocal imaging

CHO and HEK293 cells - Cells were plated on 8-well μ-slides (IBIDI) and cultured at 37°C overnight. In order to enhance channel expression, the temperature of the incubator was set to 32°C 24 hours prior to experiments. For live-cell imaging, cells were incubated with variable concentrations of ATTO488-ProTx II or Cy5-ProTx II + Hoechst (1:1,000) for 15 min on ice (although ice is not required). Cells were then rapidly washed twice and imaged in Tyrode solution (in mM: 4 KCl, 140 NaCl, 2 $CaCl_2$, 1 $MgCl_2$, 5 glucose, 10 HEPES (pH 7.4 with NaOH)) + 0.1% BSA between 10 and 30 min after washout. Confocal images were performed using a Nikon A1R confocal inverted microscope (Nikon Corp, Japan) with a Nikon X60 Plan-Apo numerical aperture (NA) 1.4 oil-immersion objective. ATTO488-ProTx II was stimulated using the 488-nm line from an argon laser. During live-cell imaging experiments, cells were maintained in a 37°C chamber, supplemented with 5% CO_2. Confocal images were analysed using ImageJ 1.52i software (Schneider, Rasband, and Eliceiri 2012).

DRG neurons - After two washes, DRG neurons were incubated in 200 nM ATTO488-ProTx II or 1 μM ATTO488-ProTx II K26E + 0.1% BSA in extracellular medium (in mM): 140 NaCl, 4 KCl, 2.5 $CaCl_2$, 1 $MgCl_2$, 10 glucose, 10 HEPES (pH 7.4 with NaOH) (all from Sigma). Cells were then rapidly washed twice and fixed 10 min with PFA 4% in PBS at RT. After 3 washes, DRG cells were stained with DAPI and finally mounted in Mowiol. Images were acquired using a LSM 780 laser-scanning confocal microscope (Zeiss), initially processed using ZEN software (Zeiss) and later exported into Adobe Photoshop (Adobe Systems) for final processing.

Cerebellar granule neurons - At DIV7, neurons were incubated with 200 nM ATTO488-ProTx II + 0.1% BSA for 10 min in PBS. Cells were then rapidly washed twice and fixed 10 min with PFA 4% in PBS at RT. After three washes, neurons were permeabilized with 0.05% Triton X100 and incubated with rabbit anti-TUJ1 antibody (1/100^e, GTX130245, GeneTex) for 1 hr at room temperature. After 3 washes, cells were stained with donkey anti-rabbit Alexa647 (1/500^e, ThermoFisher). Cells were mounted in Fluoromount-G with DAPI (Clinisciences). Images were acquired using a Nikon A1R confocal inverted microscope (Nikon Corp, Japan) with a Nikon X60 Plan-Apo numerical aperture (NA) 1.4 oil-immersion objective. Images were analyzed using ImageJ 1.53c software (Schneider, Rasband & Eliceiri, 2012).

2.6 Pull-down experiments with Biot-ProTx II

Cells were washed twice with ice-cold PBS and lysed with ice-cold lysis buffer containing 20 mM HEPES pH 7.4, 150 mM NaCl, 0.5% amidosulfobetaine-14 (zwitterionic detergent, Sigma), 1 mM phenylmethylsulfonyl fluoride (Sigma), 0.7 µg/mL pepstatin A (ThermoFisher Scientific), Complete protease inhibitor cocktail (Roche) and halt phosphatase inhibitor (ThermoFisher Scientific). After 15 min rotation at 4°C, the lysates were centrifuged at 1000g for 10 min and protein concentration was determined using Pierce BCA Protein Assay Kit (ThermoFisher Scientific). For each pull-down reaction, 200 µg of lysates was incubated with 50 µL of NeutrAvidin agarose beads (ThermoFisher Scientific) coupled to Biot-ProTx II (1 or 10 µM final concentration). After 2 hrs rotation at 4°C, the beads were washed 3 times with ice-cold lysis buffer. Proteins were eluted by adding 70 µL of 1x NuPAGE™ LDS (Lithium Dodecyl Sulfate) sample buffer (ThermoFisher Scientific) supplemented with 100 mM dithiothreitol and heating the samples for 30 min at 50°C. For each reaction, a third of the pull-down was loaded on a 4-12% acrylamide precast gel (Invitrogen) alongside 15 µg of total lysate and equivalent protein quantity for the supernatant. The samples were blotted with mouse anti-Na_VPan (Sigma, clone K58/35), GAPDH (Santa Cruz, 6C5) and/or transferrin receptor (Invitrogen, clone H68.4) antibodies. Bound primary antibodies were detected using anti-mouse secondary antibodies (Cell Signaling Technology) coupled to horseradish peroxidase, and protein signals were visualized using Super Signal West Dura Extended Duration Substrate (ThermoFisher Scientific) and a CCD camera (GE Healthcare).

2.7 Data and statistical analyses

The data and statistical analysis comply with the recommendations of the British Journal of Pharmacology on experimental design and analysis in pharmacology. Blinding of the experiments were performed on the automated patch-clamp system, the cell type and channel isoform under recording being unknown by the operator who launched the automated patch-clamp system and the compound library. Data were analysed with DataController384 V1.6.0_B9, R 3.5.1 software and GraphPad Prism 5 software. As stated in the Results section, while sample sizes were identical in most cases for each peptide and each concentration (except control condition that was repeated several times) with n=16 cells at least (independent measures), the data that were kept at each concentration were those from cells that passed two quality control checks (QC1 on seal resistance and QC2 on current density). Concentration-

response relationships were established by plotting the response, recorded in the presence of the toxin (Rt) and expressed as percentage of the value obtained in absence of toxin (Rc), against the toxin concentration ([toxin]). The theoretical concentration-response curves were calculated from sigmoid regressions through data points (correlation coefficient = r^2) according to the Hill equation: $Rt / Rc = 1 / [1 + ([toxin] / IC_{50}) n_H]$, where IC_{50} is the toxin concentration necessary to inhibit 50% of the response, and n_H is the Hill number. The $Na_v1.7$ channel conductance (G) was calculated according to the following equation: $G = I / (E_m – E_{Na})$, where I is the peak current amplitude, E_m is the test-pulse voltage, and E_{Na} is the equilibrium potential of Na^+ ions. Conductance-voltage relationships were established by plotting the conductance, expressed as percentage of the maximal conductance (Gmax), as a function of test-pulse voltage. The theoretical curves correspond to data point fits, according to the Boltzmann equation: $G / Gmax = 1 – [1 / (1 + \exp ((E_m – E_{0.5}) / k))]$, where $E_{0.5}$ is the test-pulse voltage corresponding to 50% of maximal conductance, and k is the slope of the curve. Steady-state inactivation-voltage relationships were established by plotting the peak current amplitude, expressed as percentage of the maximal amplitude (Imax) recorded at the lowest holding potential (H_P=-120 mV), as a function of holding potential. The theoretical curves correspond to data point fits, according to the Boltzmann equation: $I / Imax = 1 / [1 + \exp ((H_P – H_{P50\%}) / k)]$, where $H_{P50\%}$ is the membrane potential producing 50% maximal peak amplitude of current, and k is the slope of the curve. Data are expressed as mean ± standard deviation (S.D.) or standard errors of the mean (S.E.M.) of n different cells within one experimental condition. The statistical comparison of values was carried out with Prism 7.0 using the parametric two-tailed Student's *t*-test with Welch's correction when we don't assume S.D. equality. Differences between values were considered to be statistically significant at $P \leq 0.05$.

3 Results

3.1 Chemical synthesis of ProTx II, evaluation of the biophysical properties of CHO-hNav1.7 cells by automated patch-clamp, and pharmacological evaluation

For the synthesis of ProTx II and its fluorescent derivatives, we followed the recommendations of Park and collaborators to avoid racemization of the cysteine residues during the Fmoc solid phase synthesis (Park, Carlin, Wu, Ilyin & Kyle, 2012). **Supplementary Figure 1** illustrates the successful synthesis of ProTx II (largest RP-HPLC peak in the crude material after synthesis in **panel a**), and the successful oxidation occurring with disulphide bridge formation (shift in elution time to the left for the largest RP-HPLC peak in **panel b**, illustrating a reduction in hydrophobicity of the peptide upon folding). **Supplementary Figure 1c,d** illustrate the

effective purification of ProTx II with a monoisotopic mass of $[M+3H]^{3+}$ of 1275.5672 as determined by LC-ESI QTOF MS. This yields an experimental monoisotopic mass of 3823.68 Da, which is thus coherent with the theoretical monoisotopic mass of 3823.67 Da of oxidized ProTx II.

The next aim was to characterize the functionality of this synthetic version of ProTx II on $hNa_v1.7$ channels using the automated high-throughput patch-clamp system from Nanion (SyncroPatch 384PE). For this purpose, we used a CHO cell line stably expressing $hNa_v1.7$ and characterized first the cell properties. As shown, with the cell catch protocol that we optimized on the SyncroPatch 384PE, using the commercial single hole medium resistance plates, only 4% of the wells had either no cells attached or cells presenting seal resistances lower than 200 MΩ. In contrast, 96% of the 384 wells had cells with seal resistances above 200 MΩ with a satisfactory 81.6% of wells being above 1 GΩ (**Supplementary Figure 2a**). As a first line of quality control (QC1), we decided to keep those recordings that originated from seal resistances above 500 MΩ, thereby keeping a first set of 92% of the recordings. After applying QC1, we also examined the average CHO cell capacitance. As shown, according to the fit of the histogram, the average capacitance was 9.8 ± 3.7 pF (n=86 cells) (**Supplementary Figure 2b**). Finally, we explored the peak current distribution of $hNa_v1.7$ in these CHO cells at a test potential of 0 mV (**Supplementary Figure 2c**). This distribution was not Gaussian and illustrated rather heterogeneity in the current amplitudes. Some cells had low current amplitudes (< to 200 pA, 10.7% of cells after QC1) which is problematic for $Na_v1.7$ characterization because of CHO background currents, while others had too high current amplitudes (> to 4000 pA, 0.2% of cells) leading to space-clamp problems. As a consequence, a second quality control (QC2) was thus applied on this parameter to exclude cells with too low or, conversely, excess Na^+ currents. QC2 led to examine 89.1% of the cells remaining after QC1. Using these two QC, we next built voltage-dependent activation (representative protocol and currents in **Supplementary Figure 2d**) and steady-state inactivation curves (representative protocol and currents in **Supplementary Figure 2e**) for $hNa_v1.7$ currents (average results in **Supplementary Figure 2f**). The $hNa_v1.7$ channel has an activation threshold of -35 mV, peak current densities at +20 mV and reversal potentials above 60 mV (n=331 cells). Half-activation potential was -10.6 ± 0.6 mV (n=301), whereas the half-inactivation potential is -54.1 ± 1.3 mV (n=290). These properties define a small window current that manifests itself most between -45 and -25 mV. Once the cell line was properly characterized, we then evaluated the $Na_v1.7$ inward Na^+ current blocking properties of synthetic ProTx II (**Figure 1**). Representative current blocks of $hNa_v1.7$ currents elicited at 0 mV are shown for 1, 3.3 and 10 nM ProTx II after 2 and 13 min

of toxin application in the extracellular recording medium (**Figure 1a**). They are indicative of the potency of the toxin. No significant alterations in inactivation kinetics were observed upon application of the toxin at concentrations producing an inhibition in the range of 40 to 60% at 13 min application time (**Table I**). The kinetics of current block at 0 mV test potential are shown at various concentrations of ProTx II (**Figure 1b**) and illustrate that the time course of inhibition is toxin concentration-dependent (**Table II**). For the unmodified ProTx II, the time constants of inhibition were described by single decreasing exponentials with values ranging between 8.6 min^{-1} (3.3 nM) and 0.45 min^{-1} (333 nM) (**Table II**). We were unable to properly evaluate the time constant of toxin dissociation since the channel block by ProTx II is poorly reversible (not shown) (Park, Carlin, Wu, Ilyin & Kyle, 2012). Based on the extent of block, measured at the end of the protocol of repetitive voltage stimulations, we evaluated the IC_{50} of ProTx II-mediated $Na_v1.7$ inhibition (**Figure 1c**). A sigmoid fit through the data reveals an IC_{50} value of 1.6 ± 0.9 nM (n=51 cells) and a Hill value of h = 2.5 ± 0.4. Noticeably, the block by ProTx II is not complete with an average 8 ± 1% of current remaining at the highest concentrations (100, 333 and 1,000 nM). This may be expected for a gating modifier, as opposed to pore blockers that reach more potent blocks. Finally, it was reported in earlier studies that ProTx II has an impact on Na_v activation properties (Rajamani et al., 2017; Sokolov, Kraus, Scheuer & Catterall, 2008; Xiao, Blumenthal, Jackson, Liang & Cummins, 2010; Xu et al., 2019). We tested the effect of ProTx II on the voltage-dependence of activation at concentrations that produce between 40 and 60% current block; a condition that reliably allows evaluation of the impact of the toxin on channel properties by preserving some current. Our observations were made once block reached equilibrium. We observed a hyperpolarizing shift of the $V_{1/2}$ of activation from -10.9 ± 0.6 mV (control, n=312) to -24.5 ± 1.6 mV (ProTx II inhibition between 40 and 60%, n=20). Similarly, we also observed a hyperpolarizing shift of the steady-state inactivation curve from -56.1 ± 0.4 mV (control, n=274) to -71.8 ± 1.5 mV (ProTx II, n=19) (**Figure 1d**). While these observations are at odd of earlier ones, it should be mentioned that our protocol preserves measurable $hNa_v1.7$ currents and avoids excessive contribution of contaminating background currents; a parameter less well respected in earlier studies where the block was close to maximal. Overall, the effects led to an increase in the window current (Inset **Figure 1d**, left panel). Combined, the incomplete block by ProTx II and the increased window current, are not optimal properties for producing efficient analgesia. Adding further stringency on QC1, by selecting cells with seal resistances above 1 GΩ, did not change the nature of the observed shifts (**Supplementary Figure 3**). The hyperpolarizing shift was also observed upon

expression of β_3 in hNa$_v$1.7 cells indicating that it was β subunit-independent (**Supplementary Figure 4a**).

3.2 Impact of various chemical modifications of the N-terminus of ProTx II on oxidative folding and pharmacology of the peptide

We synthesized several novel analogues of ProTx II by modifying the N-terminus of the peptide sequence because it turns out to represent an excellent position for chemical modifications according to the topology of ProTx II binding onto the voltage sensor domain II of Na$_v$1.7 (Xu et al., 2019). As the C-terminus of ProTx II is essentially important for its activity, including the C-terminal amidation (Park et al., 2014), this part of the toxin should be left unmodified. ProTx II is notoriously difficult to fold and many earlier attempts have reportedly led to erroneously folded compounds (Wright, 2015). Therefore, before envisioning the chemical grafting of a bulky chromophore at the N-terminus of ProTx II, we performed a first round of chemical syntheses to test the impact of the N-terminus modification: first by either biotinylation of the N-terminus or second by elongating the N-terminus with an 8-amino acid-long histidine tag. The analytical RP-HPLC and MS profiles illustrate the chemical purities of the synthetic biotinylated ProTx II (Biot-ProTx II) and His-tagged ProTx II (8His-ProTx II) (**Supplementary Figure 5**). Proper molecular weights of 4049.7433 Da for Biot-ProTx II (monoisotopic mass) and of 5188.23 Da for 8His-ProTx II, as determined by LC-ESI-QTOF MS measurements, suggest a correct synthesis and oxidative folding. Again, representative current blocks of hNa$_v$1.7 currents elicited at 0 mV were shown for 1, 3.3 and 10 nM Biot-ProTx II and 8His-ProTx II after 2 and 13 min bath application of the peptides (**Figure 2a**). Again, both toxins preserved normal hNa$_v$1.7 channel inactivation kinetics (**Table I**). While the potency of Biot-ProTx II seems preserved in comparison to ProTx II (**Figure 1**), the efficacy of 8His-ProTx II seemed slightly lower, as best evidenced at 3.3 and 10 nM concentrations. To get a clearer idea of the differences in efficacies between these two analogues, we also evaluated the kinetics of current block at 0 mV test potential at various concentrations of Biot-ProTx II (**Figure 2b**) and 8His-ProTx II (**Figure 2c**). There appeared some interesting differences in the onset of current block between these two peptides. The kinetics of Biot-ProTx II-mediated current block were very similar to those of ProTx II blocks shown in **Figure 1b** with time constant ranging between 2.5 min^{-1} (3.3 nM) and 0.22 min^{-1} (333 nM) (**Table II**). In contrast, in the case of 8His-ProTx II, there was a surprising almost instantaneous block of Na$_v$1.7 Na^+ currents at all concentrations that was either maintained at a plateau level for the lowest concentrations (from 1 to 10 nM) or that could be followed by a second slower phase of block

at the highest concentrations (from 33 nM to 1 μM) (**Figure 2c**). The data are hard to interpret but suggest that the His tag contributes to a faster binding of the toxin onto the channel in one of its conformation and possibly to a slower one in another channel conformation, in agreement with the concept of a differential affinity of the toxin for each channel state (activated and deactivated (Xu et al., 2019)). Alternatively, it may reflect changes in the normal rate of lipid membrane partitioning of the toxin owing to the presence of a potentially charged His sequence at the N-terminus. We rule out the concept that the block by 8His-ProTx II is linked to a divalent cation coordination issue by the His tag since we observed exactly the same properties with Cy5-ProTx II block, as detailed later. These data inform thus that the chemical nature of the tag or its size may influence the binding properties of the toxin onto the channel in agreement with the complex chain of molecular events that are required for channel inhibition by the toxin. Evaluation of the dose-dependent block of Na^+ currents further reveal the differences between these two peptides with a slight reduction in affinity of 8His-ProTx II for $Na_v1.7$ in these cells (**Figure 2d**). The measured IC_{50} values were 0.6 ± 1.2 nM (Biot-ProTx II, n=54 cells) with a Hill value of h = 1.7 ± 0.4 and 9.7 ± 1.2 nM (8His-ProTx II, n=55 cells) with a Hill value of h = 1.1 ± 0.2. Here again, the block of $hNa_v1.7$ current by these analogues was never complete. On average, 12.1 ± 1.9% (Biot-ProTx II) and 6.9 ± 0.9% (8His-ProTx II) of the $hNa_v1.7$ currents remained unblocked at the two highest concentrations (333 nM and 1 μM). These first set of data thus illustrate that it is possible to modify the N-terminus of ProTx II without altering the oxidative folding of the peptide. Both the Biot-ProTx II and 8His-ProTx II appear to represent interesting tools to perform biochemical experiments such as channel pull-down or purification. To test their utility, we used Biot-ProTx II to perform pull-down experiments of the $hNa_v1.7$ channel. Both lysates of control CHO cells and $hNa_v1.7$-expressing CHO cells were incubated with 10 μM Biot-ProTx II immobilized on agarose NeutrAvidin beads. The amount of $hNa_v1.7$ precipitated was revealed by Western blot with an anti-Na_vPan antibody. As shown, Biot-ProTx II successfully precipitated the $hNa_v1.7$ channel from the lysate used for this pull-down (**Figure 2e**). Comparing the amount of $Na_v1.7$ in the total and supernatant fractions, we quantified that 72% of the channel could be depleted in these conditions. The specificity of this pull-down experiment is demonstrated by the absence of transferrin receptor in pull-down and highly diminished quantities of GAPDH in the pull-down (less than 8% remaining). Using several cell lines selectively expressing other hNa_v isoforms ($hNa_v1.1$, $hNa_v1.2$, $hNa_v1.3$ and $hNa_v1.6$), we evaluated whether Biot-ProTx II could be considered as a tool for selective pull-down of the $Na_v1.7$ isoform in a more complex situation (i.e. neuronal tissue expressing several sodium

channels). We illustrate that we could observe a selective, but partial, pull-down of $hNa_v1.7$ at 1 μM Biot-ProTx II (**Supplementary Figure 6a**). In contrast, at 10 μM Biot-ProTx II, the peptide acts as a pan-Na_v tool by producing an efficient pull-down of all tested hNa_v isoforms (**Supplementary Figure 6b**). The requirement of high concentrations of Biot-ProTx II for the pull-down of $hNa_v1.7$ illustrates that there remains progress to be made in experimental conditions (solubilization, peptide/channel coupling) and possibly peptide design to fully preserve the high affinity ProTx II binding site after solubilization and to reach the conditions for improved selectivity over other Na_v channel isoforms. Nevertheless, all these experiments demonstrate that the added functionalities onto ProTx II help extending its usefulness towards new applications. The relative preservation of the binding properties of the peptide onto $hNa_v1.7$ indicates that it should be feasible to produce fluorescent analogues of ProTx II.

3.3 New fluorescent ProTx II analogues as high affinity blockers of the $Na_v1.7$ channel

To chemically synthesize fluorescent analogues of ProTx II, we used click chemistry as a strategy to add a fluorescent tag onto ProTx II. To this aim, we synthesized ProTx II in its folded/oxidized form with a pentynoic acid (PAM) at the N-terminus, resulting in a new analogue with a monoisotopic mass of 3903.69 Da that was used essentially for tagging the toxin (**Supplementary Figure 7**). We already validated this approach previously on BeKm-1 (Vasseur, 2019) and for 8His-ProTx II since the His tag was added by click chemistry also (see the *Methods* section). The observation that 8His-ProTx II differed in blocking properties compared to Biot-ProTx II was an incentive to try different fluorescent dyes to best recapitulate the properties of unmodified ProTx II. Two fluorescent tags were chosen that differ by size, emission spectra, hydrophobicity and the chemical nature of the linker: Cy5-azide and ATTO488-azide. **Figure 3a** shows the sequence of the pentynoic acid-modified ProTx II (PAM-ProTx II) and the click reaction used to graft ATTO488-azide or Cy5-azide (depicted in **Figure 3b**) to PAM-ProTx II resulting in either ATTO488-ProTx II or Cy5-ProTx II production. The same strategy was conducted to graft ATTO488-azide to PAM-ProTx II K26E mutant. As seen, purified ATTO488-ProTx II eluted earlier than PAM-ProTx II by analytical RP-HPLC (**Figure 3c**) indicating decreased hydrophobicity, while the opposite was true for Cy5-ProTx II hinting for increased hydrophobicity (**Figure 3d**). LC-ESI QTOF MS illustrates that the added fluorescent tags resulted in the proper compounds ($[M+3H]^{3+}$ = 1490.3705 and hence a monoisotopic mass of 4469.0569 Da for Cy5-ProTx II and $[M+3H]^{3+}$ = 1565.3092 and a monoisotopic mass of 4693.909 Da for ATTO488-ProTx II) (**Figure 3e**) indicating that the click chemistry preserved the intact folded/oxidized state of PAM-ProTx II. This strategy of

chemical grafting after folding/oxidation avoids the inherent risks of toxin misfolding if grafting had occurred on the non-folded/oxidized version of PAM-ProTx II. Next, these two compounds were tested for hNa_v1.7 current block and their affinities compared to that of ProTx II (**Figure 4**). As shown by representative current traces at three different concentrations of the fluorescent analogues (10, 33 and 100 nM for Cy5-ProTx II (top panel of **Figure 4a**) and 1, 3.3 and 10 nM for ATTO488-ProTx II (lower panel)), the block of Na^+ current by all these compounds resulted in peak current alterations without major kinetic changes in channel inactivation (**Table I**). The only significant variation we observed was for ATTO488-ProTx II for which we noticed slightly faster channel inactivation kinetics. From these representative traces, it was evident that ATTO488-ProTx II was a better blocker than Cy5-ProTx II, and resembled in many respect the block observed for ProTx II itself (**Figure 1A**) and Biot-ProTx II (**Figure 2a**). This observation was further reinforced by examining the average kinetics of current block at various concentrations of these peptides (**Figure 4b,c**). As shown, ATTO488-ProTx II behaved more like ProTx II or Biot-ProTx II (**Figure 4b**), while Cy5-ProTx II produces Na_v1.7 current blocks with kinetics reminiscent of what we observed for 8His-ProTx II (**Figure 4c**). Concerning ATTO488-ProTx II, time constants for current block ranged between 14.9 min^{-1} (3.3 nM) and 0.7 min^{-1} (100 nM) (**Table II**). In contrast, for Cy5-ProTx II, a more complex behaviour was again observed. Indeed, the kinetic of block at 333 nM, for instance, is symptomatic of this process: it contains a component of almost instantaneous block (>50%) and a second much slower component of block (time constant quantified in **Table II**), as if the channel was in two different states at the onset of block (**Figure 4b**). The second component of block by Cy5-ProTx II was particularly slow for this analogue (**Table II**), even though part of the discrepancy can be explained by a shift in the affinity compared to ProTx II. Interestingly, the proportion of fast component of Cy5-ProTx II-mediated block increases with peptide concentration suggesting a form of cooperativity among the channels. An earlier study had demonstrated that Na_v channels can form dimers (Clatot et al., 2017), but how this may affect pharmacology is still unknown. Again, it exemplifies how chemical toxin modifications can impact its blocking properties. It is possible that the more hydrophobic fluorescent Cy5 tag excessively facilitates lipid partitioning and adds a new constrain for the accessibility to the binding site, thereby altering the regular toxin orientation in the lipid bilayer for toxin binding onto the Na_v1.7 site. Such an explanation would both explain the concentration-dependence of the increased proportion of the very fast blocking component and the rather slower kinetics of the slower blocking component. Nevertheless, in the absence of clear mechanistic understanding, it should be mentioned that the mechanism controlling these unusual kinetic behaviours are not

necessarily identical for 8His-ProTx II and Cy5-ProTx II. Plotting the extent of current inhibition of toxin block at the end of the application protocol (14 min application) indicates that Cy5-ProTx II has a lower apparent affinity than ProTx II, while ATTO488-ProTx II preserves a remarkably good IC_{50} value for $Na_v1.7$ (**Figure 4d**). While the IC_{50} value for Cy5-ProTx II was lower than ProTx II itself (14.0 ± 1.1 nM, n=52 cells *versus* 1.6 ± 1.1, n=51 cells), it remained good. It should be emphasized however that the IC_{50} value of Cy5-ProTx II is underestimated to some extent because inhibition by the lowest concentrations did not reach equilibrium at the end of a 14-min application. Longer application times were not attempted to avoid $Na_v1.7$ channel run-down that interfere with the results. For both toxins, a fraction of the current remained at maximum toxin concentration (13.1 ± 2.5% for Cy5-ProTx II (average of 3 concentrations: 333 nM, 1 μM and 10 μM) and 9.4 ± 1.2% for ATTO488-ProTx II (average of 3 concentrations: 100 nM, 333 nM and 1 μM). Nevertheless, it remains true that the best fluorescent analogue is indubitably ATTO488-ProTx II with an IC_{50} of $hNa_v1.7$ current block of 2.3 ± 1.07 nM (n=53 cells), which is fully similar to the native compound. For all these compounds, the Hill number is close to 2 (1.74 for Cy5-ProTx II and 2.05 for ATTO488-ProTx II), providing additional evidence for cooperativity in ProTx II block. Whether this cooperativity arises from the existence of two binding sites on $Na_v1.7$, as suggested by an earlier study (Shen et al., 2019), or from the interaction between a dimer channel cluster, remains to be determined. However, it appears that binding of one peptide to its site facilitates the binding of another peptide on a neighbouring site of the same channel or on a neighbouring $Na_v1.7$ channel.

3.4 Several features of ProTx II block of $Na_v1.7$ are preserved with the tagged analogues

Other characteristic features of ProTx II regulation of $hNa_v1.7$ currents were investigated as well. ProTx II shifts the voltage-dependence of activation and inactivation (**Figure 1d**). We confirmed that ATTO488-ProTx II preserves to some extent this property as well (**Figure 4e**). The observed extent of shift in activation was reduced with a half activation potential shifting from -10.9 ± 0.6 mV (control, n=312 cells) to -14.4 ± 1.4 mV (40-60% ATTO488-ProTx II inhibition, n=23 cells) instead of -24.5 ± 1.6 mV for ProTx II (**Figure 1d**). Conversely, the extent of the shift in half-inactivation was better preserved with a shift from -56.1 ± 0.4 mV (before toxin, n=274 cells) to -66.6 ± 1.3 mV (ATTO488-ProTx II, n=18 cells) (**Figure 4e**) compared to -71.8 ± 1.5 mV for ProTx II (**Figure 1d**). Combined, these two shifts produced by ATTO488-ProTx II result also in an increase of the window current at physiological voltages

between -55 and -35 mV (**Inset Figure 4e**). Again, this shift was β-subunit independent as the expression of β_3 in $hNa_v1.7$ cells preserved this shift induced by ATTO488-ProTx II (**Supplementary Figure 4b**).

Finally, we also tested whether the nature of the tag added onto ProTx II could affect the preferred selectivity for $hNa_v1.7$ channel over the other Na_v channel isoforms (**Supplementary Figure 8**). The tags did impact IC_{50} values of ProTx II block differently among the various Na_v isoforms. The biotin tag was probably one of the most conservative tag in terms of activity compared to untagged ProTx II. Variations in IC_{50} values were limited for most Na_v isoforms (3.5-fold reduction in IC_{50} value for $hNa_v1.1$ and a 1.7-fold decrease for $hNa_v1.5$) (**Supplementary Table I**). Nevertheless, there was a surprising 7.2-fold increase in apparent affinity for $hNa_v1.4$ with the biotin tag, suggesting that $hNa_v1.4$ block was sensitive to the nature of the tag at the N-terminal position of ProTx II. Interestingly enough, the Cy5 tag had the greatest impact on $hNa_v1.7$ and $hNa_v1.2$ (8.7- and 4.6-fold increases in IC_{50} value, respectively), while globally having much less impact on the other channel isoforms (between 1.6-fold increase for $hNa_v1.5$ and 2.5-fold for $hNa_v1.4$). In the case of the ATTO488 tag, the best IC_{50} value was still observed for $hNa_v1.7$ (1.4-fold increase in IC_{50} value), but this particular tag had a dramatic effect on the activity of ProTx II onto $hNa_v1.4$ (11.7-fold increase in IC_{50} value). This is coherent with the suspected sensitivity of $hNa_v1.4$ to alterations in the N-terminus seen with the biotin tag, although, in this case, the impact is diametrically opposed. For that matter, it is surprising that the Cy5 tag did not impact to a greater extent the activity of ProTx II on $hNa_v1.4$. Noticeably, $hNa_v1.1$ was quite sensitive to the presence of the ATTO488 tag (6.1-fold increase in IC_{50}). Besides these two channel types ($hNa_v1.1$ and $hNa_v1.4$), the other channels preserved a good selectivity with ATTO488. Concerning this tag, the channel that showed the highest sensitivity to ATTO-ProTx II, besides $hNa_v1.7$, was the $hNa_v1.3$ channel type (13-fold higher IC_{50} value compared to $hNa_v1.7$). Globally, the channels that were the most sensitive to the N-terminal tagging of ProTx II, by rank order of importance, were: $hNa_v1.4$ > $hNa_v1.7$ > $hNa_v1.1$ > $hNa_v1.2$. $hNa_v1.5$ and $hNa_v1.6$ were the least affected. Unfortunately, ProTx II itself and its analogues could not be tested on $hNa_v1.8$ and $hNa_v1.9$ because of difficulties in expression and lack of availability of cell lines expressing these isoforms.

3.5 The fluorescent ProTx II analogues efficiently label $Na_v1.7$ channels at the cell surface

Since one possible application of fluorescent ProTx II analogues is to be used in a similar manner than anti-$Na_v1.7$ antibodies, we next assessed whether these fluorescent ProTx II peptides could be used to label the $hNa_v1.7$ channel. Cultured control CHO and $hNa_v1.7$-

expressing CHO cells were incubated 15 min with 1 μM ATTO488-ProTx II and rapidly (within 10-30 min) imaged by confocal microscopy (**Figure 5**). At low magnification (x200) and using identical settings for CHO and hNa$_v$1.7-CHO cells, ATTO488-ProTx II specifically labels CHO cells expressing hNa$_v$1.7 and not control CHO cells (**Figure 5a**). The fluorescence intensity was variable from cell to cell, reflecting the observed variability in current amplitudes for this stable cell line (**Supplementary Figure 2c**). At higher magnification (x600), ATTO488-ProTx II appears to remain confined mainly to the plasma membrane of hNa$_v$1.7-CHO cells, indicating that the fluorescent peptide does not cross the membrane, contrary to some other toxins (Boisseau et al., 2006; Mabrouk et al., 2007; Ram et al., 2008a; Ram et al., 2008b) (**Figure 5b**). Quantification of this fluorescence on representative cells illustrate that ATTO488 fluorescence does not overlap with the Hoechst labelling and confirms the absence of fluorescence on CHO cells. Orthogonal views (xz and yz) of the stacked confocal images also indicate that the ATTO488 fluorescence confines to the plasma membrane of hNa$_v$1.7-CHO cells only (**Figure 5c**). Similar findings were obtained if cells were fixed with 4% paraformaldehyde (PFA) after labelling the cells 15 min with 200 nM ATTO488-ProTx II and two washes (**Supplementary Figure 9**). Labelling control CHO and hNa$_v$1.7-CHO cells with ATTO488-ProTx II after PFA fixation leads to non-specific fluorescence marking into the cytoplasm making hNa$_v$1.7 labelling more challenging (data not shown). Of interest was the fact that a specific labelling of hNa$_v$1.7 was also possible using Cy5-ProTx II as a tool, in spite of its higher hydrophobicity and lower blocking affinity (**Supplementary Figure 10**). To further assess the specificity of hNa$_v$1.7 labelling by ATTO488-ProTx II, the most potent fluorescent analogue of ProTx II, we assessed whether this peptide could label the other Na$_v$ isoforms expressed in HEK293 or CHO cells. As shown, 200 nM ATTO488-ProTx II was unable to specifically label any of the Na$_v$ channel isoforms that we tested (from hNa$_v$1.1 to hNa$_v$1.6; **Supplementary Figure 11a**). hNa$_v$1.4 was not tested since it was by far the least sensitive isoform to ATTO488-ProTx II (**Supplementary Table I**). At a higher concentration (1 μM), a small percentage of hNa$_v$1.3 and hNa$_v$1.6-expressing cells could be labelled by ATTO488-ProTx II, but other hNa$_v$ channels remained undetectable. The hNa$_v$1.3 detection at 1 μM is coherent with the fact that this channel type is the second most sensitive to ATTO488-ProTx II application (**Supplementary Figure 8c**). As a positive control, all these cell lines showed evident cell surface expression of Na$_v$ channels as testified from automated patch-clamp recordings from a great number of cells (**Supplementary Figure 11b**). A further test of Na$_v$-labelling selectivity of ATTO488-ProTx II was performed by incubating the peptide with

primary cultures of cerebellar granule cells at 7 DIV. The cerebellar cortex does not express the $Na_v1.7$ isoform and we indeed confirm that Tuj1-positive neurons fail to be labelled by 200 nM ATTO488-ProTx II (**Supplementary Figure 11c**). From these experiments, it was clear that at 200 nM ATTO488-ProTx II specifically labels $hNa_v1.7$ over the other types of Na_v tested herein. It will be interesting to test in the future lower concentrations than 200 nM for an additional gain in selectivity and, also, higher ones to use this analogue as a PAN-Na_v marker. In all these tests, fluorescence could be observed between 10 to 30 min after labelling which is coherent with the slow off-rate of the peptide from the channel. Longer washout times might be tested to see how durable fluorescence is kept at the cell surface. To test the applicability of this new fluorescent tool for primary neurons, we labelled live mouse DRG neurons grown 2 DIV with 200 nM ATTO488-ProTx-II, fixed them with 4% PFA and labelled the nucleus with DAPI. This concentration was shown to minimize any off-target labelling as shown on our validation tests on CHO or HEK293 cells. Here again, the DRG neuron was labelled at the level of the plasma membrane only, as evidenced by the image and the quantification (**Figure 5d**). Noticeably, at this stage, only the soma of DRG neurons were found to be labelled as well as the proximal part of the neurite, indicating an asymmetric distribution of ProTx II receptors at the surface of the DRG neuron. At 4 DIV, the neurites were found to be labelled as well (**Supplementary Figure 12a**). While it would be of interest to assess the change in labelling of preparations devoid of $Na_v1.7$ expression, using knockout mice for $Na_v1.7$ for instance, we cannot rule out that the peptide also labels other Na_v isoforms, such as $Na_v1.8$, $Na_v1.9$ against which ProTx II was never tested as far as we know, or any other additional unknown off-targets such as voltage-gated potassium channels. To further confirm that ATTO488-ProTx II indeed labels $Na_v1.7$ channel in DRG neurons, we chemically synthesized the ATTO488-ProTx II K26E variant. Earlier structure-function relationship studies indicated that this mutation altered by over 10,000-fold the IC_{50} for $Na_v1.7$ channel block (Xu et al., 2019). In agreement, all surface labelling of DRG neurons were lost at both 200 nM and 1 μM ATTO488-ProTx II K26E concentrations (**Supplementary Figure 12b**). This indicates that this ProTx II mutant comes as an important negative control to assess the specificity of $Na_v1.7$ labelling in neuronal tissues.

3.6 Use of ATTO488-ProTx II in cell sorting experiments and voltage-dependence of toxin binding on $hNa_v1.7$

To get a better grip on how effective ATTO488-ProTx II is to label $hNa_v1.7$ at low concentrations, we also quantified by cell sorting experiments the fluorescence at the surface of CHO and $Na_v1.7$-CHO cells incubated with different concentrations of ATTO488-ProTx II

(**Figure 6a**). The gating conditions are provided in **Supplementary Figure 13**. At concentrations up to 1 μM, no specific labelling could be observed on control CHO cells. However, there was a distinctive and homogeneous labelling of $hNa_v1.7$-CHO cells occurring at 300 nM ATTO488-ProTx II that was further enhanced using 1 μM ATTO488-ProTx II. It may seem curious that the dose-response used to block $hNa_v1.7$ in CHO cells is shifted leftward compared to the doses required to label the cells in imaging and biochemistry experiments. We tentatively explain this discrepancy by the fact that ProTx II block is highly voltage-dependent with a reported 60-fold lower affinity at a holding potential of 0 mV versus -120 mV (Xu et al., 2019). Indeed, in our patch-clamp experiments, the holding potential of $hNa_v1.7$-CHO cells was positioned at -100 mV, while non-clamped CHO cells, used for imaging, have most likely a very depolarized membrane potential (close to -20 / 0 mV). Next, we determined whether cell fluorescence analysis could be used to examine the effect of compounds in displacing ATTO488-ProTx II fluorescence at the surface of $hNa_v1.7$-CHO cells (**Figure 6b**). As shown, a 20-min preincubation of $hNa_v1.7$-CHO cells with 10 μM ProTx II led to a significant 65% decrease in fluorescence associated with a subsequent 20-min incubation with 2 μM ATTO488-ProTx II. This result indicates that, theoretically, it should be possible to screen for small compounds that displace ProTx II from its binding site on $hNa_v1.7$ by simply using a cell analyser. These compounds may in turn possess more favourable *in vivo* drug characteristics. The main advantage of performing these experiments with a cell sorter is that the toxin does not have to be washed away from the solution as the measure of fluorescence is limited to the bound fraction. This implies that we do not have to worry about reversible association; although this is not a major concern in the case of ProTx II.

4 Discussion and Conclusion

By using peptide engineering, we managed to produce several analogues of ProTx II that preserve several of the pharmacological properties of ProTx II. This was not an obvious challenge considering the mechanistic complexities involved in accessing the binding site (that requires lipid partitioning) and in blocking the channel (that is largely voltage-dependent). The recent structural elucidation of the molecular basis of interaction and block of $Na_v1.7$ by ProTx II provided a helpful guideline in deciding that the amino terminus of ProTx II is a convenient locus for grafting new chemical modalities onto ProTx II (Xu et al., 2019). However, our observation that several of the tags, all positioned at this N-terminal position, modified, to some extent, both the kinetics and IC_{50} of ProTx II-mediated $Na_v1.7$ current block, but also the Na_v

selectivity, comes as a reminder that the nature of these tags may sterically hinder proper lipid partitioning, 2D positioning in the membrane and receptor site engagement. In an even more dynamic perspective, ProTx II being a gating modifier, the tag hindrance factor of ProTx II channel may as well depend on the channel state itself (closed *versus* activated or inactivated). The membrane potential level of the cell could potentially reconfigure the toxin position within the lipid interface and the nature of its interaction with the channel depending on the tag identity grafted at the N-terminus of ProTx II. In spite of these potential pitfalls, two analogues were shown to have properties almost indistinguishable of the native ProTx II (Biot-ProTx II and ATTO488-ProTx II), while two others still preserved good affinities (8His-ProTx II and Cy5-ProTx II) and remain interesting molecular tools to use. Both fluorescent analogues, in spite of differences in chemical properties, proved useful for a specific labelling of $Na_v1.7$ channels over several other Na_v isoforms in cell sorting experiments (tested for ATTO488-ProTx II) and confocal imaging (tested with both toxins). The demonstrated possibility to produce various ProTx II analogues that differ by their tag fluorescence properties, along with the observed differences in IC_{50} values recorded for various Na_v isoforms, indicates that, theoretically, it should be feasible to label specifically $Na_v1.7$ with one given fluorescent ProTx II and another Na_v isoform of lower affinity with yet a different fluorescent ProTx II analogue. A logical follow-up study will be the use of these fluorescent ProTx II analogues on sectioned material to investigate the distribution of $Na_v1.7$ channels in DRG neurons. It would nicely complement an elegant investigation of the channel trafficking properties in DRG neurons that confirmed the impact of inflammation on $Na_v1.7$ trafficking and membrane distribution through the use of engineered tagged channels (Akin et al., 2019). The use of fluorescent peptides would be useful to extend these findings and confirm them in a context where only native $Na_v1.7$ channels are studied, hence avoiding potential flaws associated with channel tagging and expression systems. To be meaningful these studies should make use of negative control peptides (such as the K26E mutant that no longer bind $Na_v1.7$ and that illustrates the specificity of labelling) and the use of $Na_v1.7$ knockout animals.

The absence of control CHO cell labelling by ATTO488-ProTx II or Cy5-ProTx II may seem surprising since lipid partitioning is a critical priming step for ProTx II binding to occur on $Na_v1.7$. We conclude that, for ProTx II and all the fluorescent analogues that were designed, the absence of a stable channel binding site in the plasma membrane precludes a steady sojourn in cell membranes. In a way, it is a reassuring observation as massive quantities of ProTx II, incompatible with therapeutic applications, would be required *in vivo* if the toxin did accumulate in the plasma membrane of cell types that are unrelated to pain neuronal processing.

The competitive inhibition of ATTO488-ProTx II binding onto $Na_v1.7$ by unlabelled ProTx II in cell sorting experiments indicates that this fluorescent analogue represents an innovative tool for drug screening campaigns aiming to identify new pharmaceutical compounds that bind onto the same site than ProTx II. Concerning Biot-ProTx II, this analogue reveals itself also as a very interesting molecular tool for affinity purification and biochemical characterization of $Na_v1.7$ channel in pull-down experiments, but also as pan-Na_v tool if the concentration is adjusted properly. According to the structural information provided by Xu and collaborators (Xu et al., 2019), there remains room for additional improvements of these new analogues. For instance, the R22Nor-arginine and the K26R mutations of ProTx II both are susceptible to further improve the IC_{50} by an order of magnitude, leaving ample room to design new ATTO488-ProTx II analogues with greater affinities. This may be required to lower the consumption of this fluorescent analogue in screening campaigns, particularly in cell lines that possess depolarized membrane potentials, a factor that greatly influences the affinity of ProTx II and ATTO488-ProTx II and leads to higher concentration requirements. However, we should emphasize that the current level of apparent affinity reached with these analogues is already quite satisfying. Conversely, to evaluate the specificity of a fluorescence staining or of a pull-down experiment, the K26E mutation is now of demonstrated interest as well as it induces over 10,000-fold loss in IC_{50} value (Xu et al., 2019) and no longer labels $Na_v1.7$ at the concentrations used herein.

A few words should be added on the analgesic potential of ProTx II that is largely debated in the literature. Two surprising observations were made that are worth discussing. The first one is that ProTx II does not fully inhibit $hNa_v1.7$ currents. This property is well preserved by ATTO488-ProTx II, but we observed that the nature of the tag can also influence this parameter. In other words, it may be possible to design optimized ProTx II analogues in the future with improved blocking properties. In our hands, it was the 8His-ProTx II analogue that behaved the best on that matter. The second more surprising result was that, at intermediate concentrations, a situation that has great likelihood to occur *in vivo*, considering the difficulties that the toxin may have to access its binding site, ProTx II and, to a lower extent ATTO488-ProTx II, shifted the voltage-dependence of activation towards more hyperpolarized potentials, hence favouring the appearance of a window current for $hNa_v1.7$, that most likely would counteract the analgesic effect expected. Overexpressing the β_3 subunit in $hNa_v1.7$ cell line led to the same results and conclusions, indicating that this shift is not β subunit-dependent. This result is at odd with earlier observations (Xiao, Blumenthal, Jackson, Liang & Cummins, 2010; Xu et al., 2019) but these authors used higher toxin concentrations. A larger set of investigations will be needed to determine the reasons for this discrepancy (possibly because we investigated

this issue at intermediate levels of ProTx II block). Whatever the exact reason, this window current, if confirmed by additional studies, should be carefully considered when investigating the analgesic potential of ProTx II.

To conclude, we demonstrate that modifying the N-terminus of ProTx II allows the generation of a new set of analogues entitled with interesting new functional properties. The ATTTO488-ProTx II appears as a particularly interesting tool to advantageously mimic $Na_v1.7$ antibodies in investigating the distribution of $Na_v1.7$ channels in neuronal tissues. Other modifications may be envisioned in the future that also have the potential to improve the analgesic properties of ProTx II.

ASSOCIATED CONTENT

Supporting information

Additional figures related to the chemical syntheses of ProTx II analogues, the RP-HPLC profiles and MS analyses, the FACS settings, additional controls for confocal imaging experiments, as well as additional biophysical and pharmacological characterizations of Na_v channels by automated patch-clamp methods are provided in Supporting information. This material is available free of charge via the internet at http://pubs.acs.org.

References

Akin EJ, Higerd GP, Mis MA, Tanaka BS, Adi T, Liu S*, et al.* (2019). Building sensory axons: Delivery and distribution of NaV1.7 channels and effects of inflammatory mediators. Sci Adv 5**:** eaax4755.

Bilimoria PM, & Bonni A (2008). Cultures of cerebellar granule neurons. CSH Protoc 2008**:** pdb prot5107.

Boisseau S, Mabrouk K, Ram N, Garmy N, Collin V, Tadmouri A*, et al.* (2006). Cell penetration properties of maurocalcine, a natural venom peptide active on the intracellular ryanodine receptor. Biochim Biophys Acta 1758**:** 308-319.

Coste B, Crest M, & Delmas P (2007). Pharmacological dissection and distribution of NaN/Nav1.9, T-type Ca2+ currents, and mechanically activated cation currents in different populations of DRG neurons. J Gen Physiol 129**:** 57-77.

Cox JJ, Reimann F, Nicholas AK, Thornton G, Roberts E, Springell K*, et al.* (2006). An SCN9A channelopathy causes congenital inability to experience pain. Nature 444**:** 894-898.

Cummins TR, Dib-Hajj SD, & Waxman SG (2004). Electrophysiological properties of mutant Nav1.7 sodium channels in a painful inherited neuropathy. J Neurosci 24**:** 8232-8236.

Dib-Hajj SD, Rush AM, Cummins TR, Hisama FM, Novella S, Tyrrell L*, et al.* (2005). Gain-of-function mutation in Nav1.7 in familial erythromelalgia induces bursting of sensory neurons. Brain 128**:** 1847-1854.

Faber CG, Hoeijmakers JG, Ahn HS, Cheng X, Han C, Choi JS*, et al.* (2012). Gain of function Nanu1.7 mutations in idiopathic small fiber neuropathy. Ann Neurol 71**:** 26-39.

Fertleman CR, Baker MD, Parker KA, Moffatt S, Elmslie FV, Abrahamsen B*, et al.* (2006). SCN9A mutations in paroxysmal extreme pain disorder: allelic variants underlie distinct channel defects and phenotypes. Neuron 52**:** 767-774.

Fischer TZ, & Waxman SG (2010). Familial pain syndromes from mutations of the NaV1.7 sodium channel. Ann N Y Acad Sci 1184**:** 196-207.

Gingras J, Smith S, Matson DJ, Johnson D, Nye K, Couture L*, et al.* (2014). Global Nav1.7 knockout mice recapitulate the phenotype of human congenital indifference to pain. PLoS One 9**:** e105895.

Hoeijmakers JG, Han C, Merkies IS, Macala LJ, Lauria G, Gerrits MM*, et al.* (2012). Small nerve fibres, small hands and small feet: a new syndrome of pain, dysautonomia and acromesomelia in a kindred with a novel NaV1.7 mutation. Brain 135**:** 345-358.

Lee JH, Park CK, Chen G, Han Q, Xie RG, Liu T*, et al.* (2014). A monoclonal antibody that targets a NaV1.7 channel voltage sensor for pain and itch relief. Cell 157**:** 1393-1404.

Li Z, Li Y, Cao J, Han X, Cai W, Zang W*, et al.* (2017). Membrane protein Nav1.7 contributes to the persistent post-surgical pain regulated by p-p65 in dorsal root ganglion (DRG) of SMIR rats model. BMC Anesthesiol 17**:** 150.

Lim TK, Shi XQ, Martin HC, Huang H, Luheshi G, Rivest S*, et al.* (2014). Blood-nerve barrier dysfunction contributes to the generation of neuropathic pain and allows targeting of injured nerves for pain relief. Pain 155**:** 954-967.

Liu D, Tseng M, Epstein LF, Green L, Chan B, Soriano B*, et al.* (2016). Evaluation of recombinant monoclonal antibody SVmab1 binding to Na V1.7 target sequences and block of human Na V1.7 currents. F1000Res 5**:** 2764.

Mabrouk K, Ram N, Boisseau S, Strappazzon F, Rehaim A, Sadoul R*, et al.* (2007). Critical amino acid residues of maurocalcine involved in pharmacology, lipid interaction and cell penetration. Biochim Biophys Acta 1768**:** 2528-2540.

Middleton RE, Warren VA, Kraus RL, Hwang JC, Liu CJ, Dai G*, et al.* (2002). Two tarantula peptides inhibit activation of multiple sodium channels. Biochemistry 41**:** 14734-14747.

Nassar MA, Stirling LC, Forlani G, Baker MD, Matthews EA, Dickenson AH*, et al.* (2004). Nociceptor-specific gene deletion reveals a major role for Nav1.7 (PN1) in acute and inflammatory pain. Proc Natl Acad Sci U S A 101**:** 12706-12711.

Nicolas S, Zoukimian C, Bosmans F, Montnach J, Diochot S, Cuypers E*, et al.* (2019). Chemical Synthesis, Proper Folding, Nav Channel Selectivity Profile and Analgesic Properties of the Spider Peptide Phlotoxin 1. Toxins (Basel) 11.

Park JH, Carlin KP, Wu G, Ilyin VI, & Kyle DJ (2012). Cysteine racemization during the Fmoc solid phase peptide synthesis of the Nav1.7-selective peptide--protoxin II. J Pept Sci 18**:** 442-448.

Park JH, Carlin KP, Wu G, Ilyin VI, Musza LL, Blake PR*, et al.* (2014). Studies examining the relationship between the chemical structure of protoxin II and its activity on voltage gated sodium channels. J Med Chem 57**:** 6623-6631.

Rajamani R, Wu S, Rodrigo I, Gao M, Low S, Megson L*, et al.* (2017). A Functional NaV1.7-NaVAb Chimera with a Reconstituted High-Affinity ProTx-II Binding Site. Mol Pharmacol 92**:** 310-317.

Ram N, Aroui S, Jaumain E, Bichraoui H, Mabrouk K, Ronjat M*, et al.* (2008a). Direct peptide interaction with surface glycosaminoglycans contributes to the cell penetration of maurocalcine. J Biol Chem 283**:** 24274-24284.

Ram N, Weiss N, Texier-Nogues I, Aroui S, Andreotti N, Pirollet F*, et al.* (2008b). Design of a disulfide-less, pharmacologically inert, and chemically competent analog of maurocalcine for the efficient transport of impermeant compounds into cells. J Biol Chem 283**:** 27048-27056.

Rusconi R, Scalmani P, Cassulini RR, Giunti G, Gambardella A, Franceschetti S, *et al.* (2007). Modulatory proteins can rescue a trafficking defective epileptogenic Nav1.1 Na+ channel mutant. J Neurosci 27**:** 11037-11046.

Schmalhofer WA, Calhoun J, Burrows R, Bailey T, Kohler MG, Weinglass AB, *et al.* (2008). ProTx-II, a selective inhibitor of NaV1.7 sodium channels, blocks action potential propagation in nociceptors. Mol Pharmacol 74**:** 1476-1484.

Schneider CA, Rasband WS, & Eliceiri KW (2012). NIH Image to ImageJ: 25 years of image analysis. Nat Methods 9**:** 671-675.

Smith JJ, Cummins TR, Alphy S, & Blumenthal KM (2007). Molecular interactions of the gating modifier toxin ProTx-II with NaV 1.5: implied existence of a novel toxin binding site coupled to activation. J Biol Chem 282**:** 12687-12697.

Sokolov S, Kraus RL, Scheuer T, & Catterall WA (2008). Inhibition of sodium channel gating by trapping the domain II voltage sensor with protoxin II. Mol Pharmacol 73**:** 1020-1028.

Tanaka K, Sekino S, Ikegami M, Ikeda H, & Kamei J (2015). Antihyperalgesic effects of ProTx-II, a Nav1.7 antagonist, and A803467, a Nav1.8 antagonist, in diabetic mice. J Exp Pharmacol 7**:** 11-16.

Torres-Perez JV, Adamek P, Palecek J, Vizcaychipi M, Nagy I, & Varga A (2018). The NAv1.7 blocker protoxin II reduces burn injury-induced spinal nociceptive processing. J Mol Med (Berl) 96**:** 75-84.

Vasseur L, Chavanieu, A., Combemale, S., Caumes, C., Béroud, R., De Waard, M., Ducrot, P., Boutin, J.A., Cens, T. (2019). Fluorescent analogues of BeKm-1 with high and specific activity against the hERG channel. Toxicon 2.

Weiss J, Pyrski M, Jacobi E, Bufe B, Willnecker V, Schick B, *et al.* (2011). Loss-of-function mutations in sodium channel Nav1.7 cause anosmia. Nature 472**:** 186-190.

Wright Z (2015). Synthesis of truncated analogues of ProTx-II as a novel form of pain relief. Doctoral thesis, University College London.

Xiao Y, Blumenthal K, Jackson JO, 2nd, Liang S, & Cummins TR (2010). The tarantula toxins ProTx-II and huwentoxin-IV differentially interact with human Nav1.7 voltage sensors to inhibit channel activation and inactivation. Mol Pharmacol 78**:** 1124-1134.

Xu H, Li T, Rohou A, Arthur CP, Tzakoniati F, Wong E, *et al.* (2019). Structural Basis of Nav1.7 Inhibition by a Gating-Modifier Spider Toxin. Cell 176**:** 702-715.

Figure legends

Figure 1. Pharmacological block of $hNa_v1.7$ by the synthetic ProTx II. (a) Representative $hNa_v1.7$ current traces elicited at 0 mV from a holding potential of -100 mV illustrating the extent of current block by various concentrations of ProTx II. (b) Average normalized time course of $hNa_v1.7$ current inhibition (mean ± S.E.M) by various concentrations of ProTx II (n= 5 to 8 cells/concentration; total n=47 cells). (c) Average dose-response curves for $hNa_v1.7$ current inhibition by ProTx II. The data were fitted according to a Hill equation. Note that inhibition leaves 8 ± 1% of unblocked current at highest concentrations (n=5 cells). (d) Effects

of ProTx II on channel activation and inactivation. Application of the toxin (blue, n=20 cells) at concentrations producing an inhibition in the range of 40 to 60%, induces significant shift of activation and inactivation curves to negative potentials compared to the condition without toxin (black, n=301 cells). Non-visible error bars are within symbol size limits. Inset: Window current shifted to hyperpolarized potentials after ProTx II application. Student *t*-test, * $p<0.05$ versus control.

Figure 2. Tagged-ProTx II analogues for biochemistry. (a) Representative $hNa_v1.7$ current traces elicited at 0 mV from a holding potential of -100 mV illustrating the extent of current block by three concentrations of ProTx II at 2 and 13 min of ProTx II analogue application. Top panel (orange): Biot-ProTx II data. Lower panel (blue): 8His-ProTx II data. (b) Average normalized time course of $hNa_v1.7$ current inhibition (mean ± S.E.M) by various concentrations of Biot-ProTx II (n= 3 to 6 cells/concentration; total number of cells recorded 32). (c) Average normalized time course of $hNa_v1.7$ current inhibition (mean ± S.E.M) by various concentrations of 8His-ProTx II (n= 3 to 8 cells/concentration; total number of cells 49). (d) Average dose-response curves for $hNa_v1.7$ current inhibition by Biot-ProTx II (n=32 cells) and 8His-ProTx II (n=49 cells). The data were fitted according to a Hill equation and yield IC_{50} values of 0.6 ± 1.2 nM (biot-ProTx II) and 9.5 ± 1.2 nM (8His-ProTx II) and nH = 1.7 ± 0.4 (Biot-ProTx II) and nH = 1.1 ± 0.2 (8His-ProTx II). Note that inhibition leaves 15% (Biot-ProTx II) or 5% (8His-ProTx II) of unblocked current at highest concentrations. (e) Pull-down using CHO-$Na_v1.7$ cells showing that 72% of the channel could be depleted using 10 µM of Biot-ProTx II.

Figure 3. Production of fluorescent analogues of ProTx II. (a) Primary structure of PAM-ProTx II indicating the disulfide bridge pattern of ProTx II and the chemical structure of PAM, coupled through peptide chemistry to the N-terminus of ProTx II. The chemical structure of ATTO488 is also shown in green, as well as the click chemistry conditions used to couple the dye to PAM-ProTx II. The blue linker contains the azide function that was added by the manufacturer onto ATTO-488. (b) Chemical structure of Cy5-azide. The Cy5 dye is in green and the linker allowing click chemistry in blue. (c) Analytical RP-HPLC demonstrating the purity of folded/oxidized ATTO488-ProTx II and its earlier elution than PAM-ProTx II, indicating that the ATTO488 dye adds hydrophilicity. (d) Analytical RP-HPLC demonstrating the purity of folded/oxidized Cy5-ProTx II and its later elution than PAM-ProTx II, indicating that, contrary to the ATTO488 dye, the Cy5 dye adds hydrophobicity. (e) LC-ESI QTOF MS illustrates that

the added fluorescent tags resulted in the proper compounds ($[M+3H]^{3+}$ = 1565.3092 for ATTO488-ProTx II (top panel) and $[M+3H]^{3+}$ = 1490.3705 for Cy5-ProTx II (lower panel)).

Figure 4. Pharmacological properties of fluorescent ProTx II analogues. (a) Representative $hNa_v1.7$ current traces elicited at 0 mV from a holding potential of -100 mV illustrating the extent of current block by various concentrations of Cy5-ProTx II (top panel, red) and ATTO488-ProTx II (lower panel, green) at 2 and 13 min peptide application time. (b) Average normalized time course of $hNa_v1.7$ current inhibition (mean ± S.E.M) by various concentrations of Cy5-ProTx II (n= 5 to 8 cells/concentration; total cells of 45). (c) Average normalized time course of $hNa_v1.7$ current inhibition (mean ± S.E.M) by various concentrations of ATTO488-ProTx II (n= 6 to 8 cells/concentration; total of 47 cells). (d) Average dose-response curves for $hNa_v1.7$ current inhibition by Cy5-ProTx II (n=45 cells total) and ATTO488-ProTx II (n=47 cells total). Fit of the data yield IC_{50} values of 14.5 ± 1.1 nM (Cy5-ProTx II) and 2.3 ± 1.1 nM (ATTO488-ProTx II) and nH = 1.7 ± 0.3 (Cy5-ProTx II) and nH = 2.1 ± 0.2 (ATTO488-ProTx II). Note that inhibition leaves 11% (Cy5-ProTx II) or 8% (ATTO488-ProTx II) of unblocked current at highest concentrations. (e) Effects of ATTO488-ProTx II on channel activation and inactivation. Application of the toxin (green, n=26 cells) at concentrations producing an inhibition in the range of 40 to 60%, induces significant shift of inactivation curve to negative potentials compared to the condition without toxin (black, n=301 cells). Non-visible error bars are within symbol size limits. Inset: Window current shifted to hyperpolarized potentials after ProTx II application. Student t-test, * $p<0.05$ versus control.

Figure 5. ATTO488-ProTx II specifically labels $Na_v1.7$-expressing CHO cells. (a) Large scale mosaic images showing labelling of live CHO-$Na_v1.7$ (lower panel) but not CHO colonies (upper panel) in the presence of 1 µM ATTO488-ProTx II (green). Nuclei were stained with Hoechst (blue). Scale bars represent 100 µm. (b) x60 magnification of CHO (upper left) and CHO-$Na_v1.7$ (upper right) cells treated with 1 µM ATTO488-ProTx II. Scale bars represent 20 µm. Red cell-crossing lines were used to plot fluorescence in both conditions (bottom). (c) Orthogonal views of CHO and CHO-$Na_v1.7$ labelled cells. Dashed lines represent orthogonal cuttings used to obtain xz and yz projections (bottom and right of the corresponding image respectively). (d) A typical mouse 2 DIV DRG neuron labelled with 200 nM ATTO488-ProTx II (brightfield image, labelling with DAPI, labelling with ATTO488-ProTx II and merge image)

are shown. Scale bar 15 μm. The red cell-crossing line was used for fluorescence quantification (right panel).

Figure 6. Specificity of ATTO488-ProTx II on CHO cells. (a) Representative histograms of CHO or CHO-$Na_v1.7$ cells incubated for 20 min with 300 nM or 1 μM of ATTO488-ProTx II at room temperature analysed by flow cytometry for total FITC-A. Fluorescence intensity is increased by toxin application only in CHO-$Na_v1.7$ cells. (b) Preincubation of CHO-$Na_v1.7$ cells with 10 μM non-fluorescent ProTx II decreases $Na_v1.7$ availability for 2 μM ATTO488-ProTx II.

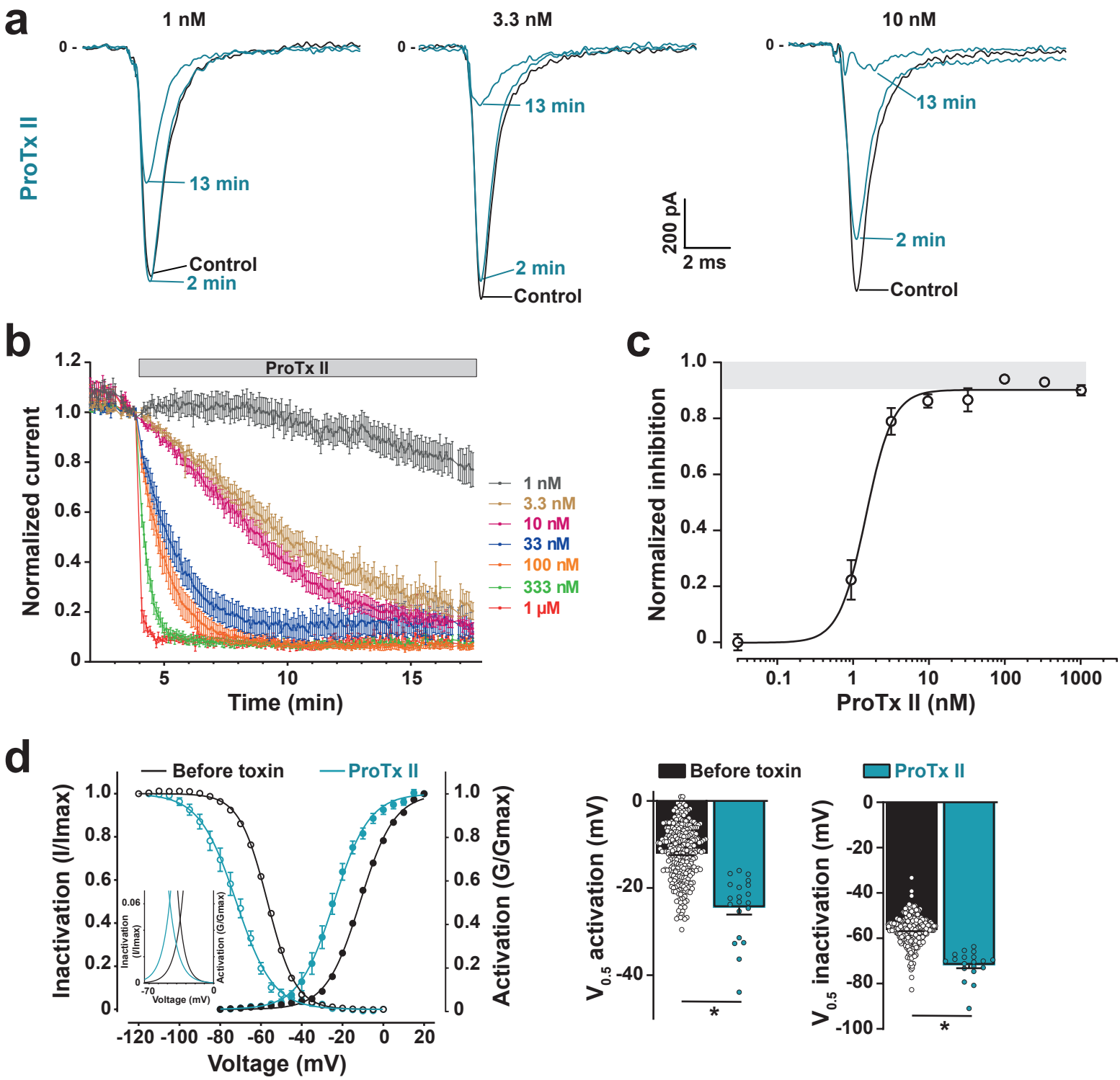
a
1 nM
3.3 nM
10 nM
ProTx II
0
13 min
Control
2 min
200 pA
2 ms
b
ProTx II
Normalized current
Time (min)
1 nM
3.3 nM
10 nM
33 nM
100 nM
333 nM
1 µM
c
Normalized inhibition
ProTx II (nM)
d
Before toxin
ProTx II
Inactivation (I/Imax)
Activation (G/Gmax)
Voltage (mV)
V0.5 activation (mV)
V0.5 inactivation (mV)

Figure 1

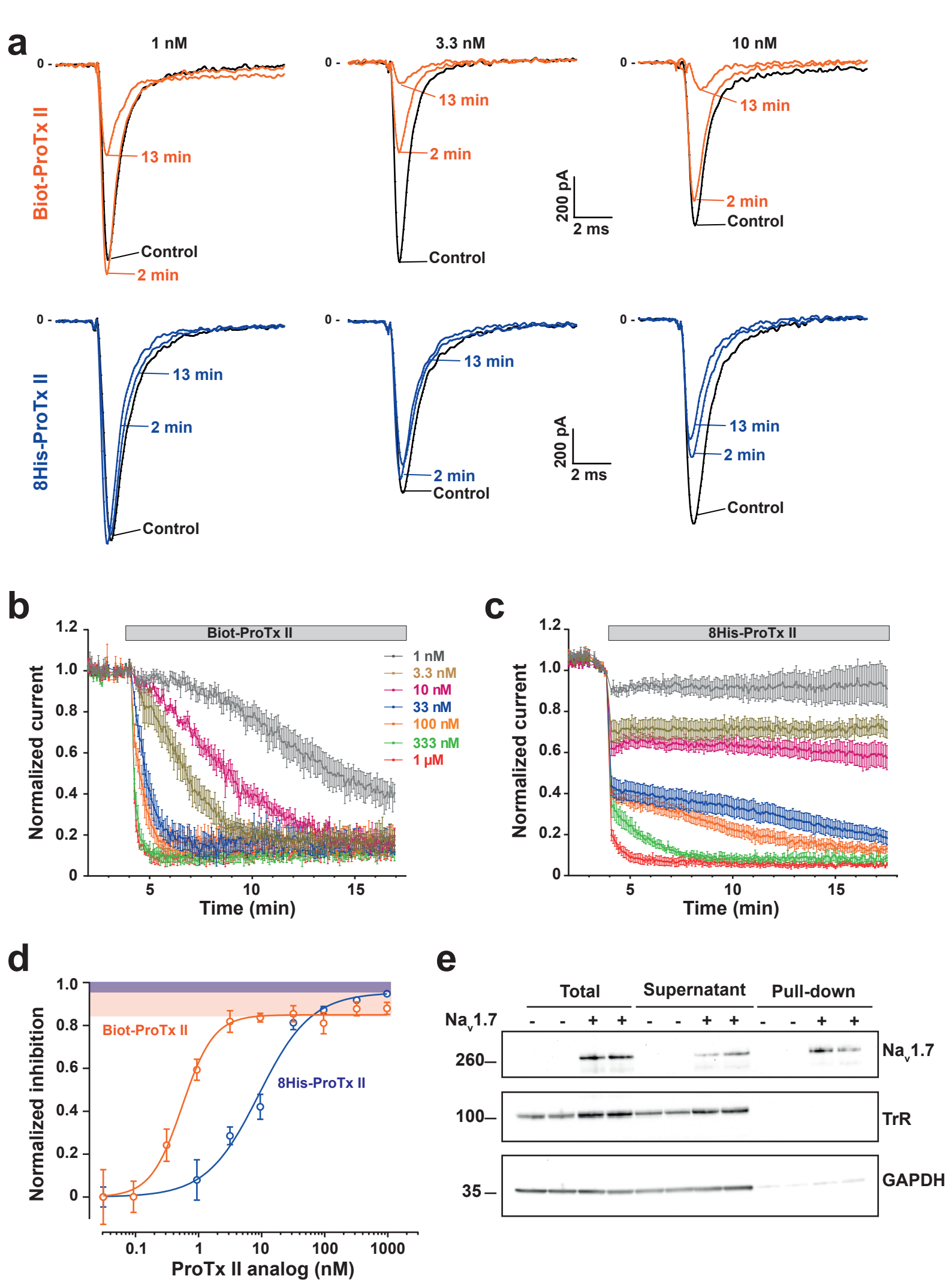
a
1 nM
3.3 nM
10 nM
Biot-ProTx II
8His-ProTx II
0
13 min
2 min
Control
200 pA
2 ms
b
Biot-ProTx II
1 nM
3.3 nM
10 nM
33 nM
100 nM
333 nM
1 µM
Normalized current
Time (min)
c
8His-ProTx II
Normalized current
Time (min)
d
Biot-ProTx II
8His-ProTx II
Normalized inhibition
ProTx II analog (nM)
e
Total
Supernatant
Pull-down
Na$_v$1.7
260
100
35
TrR
GAPDH

Figure 2

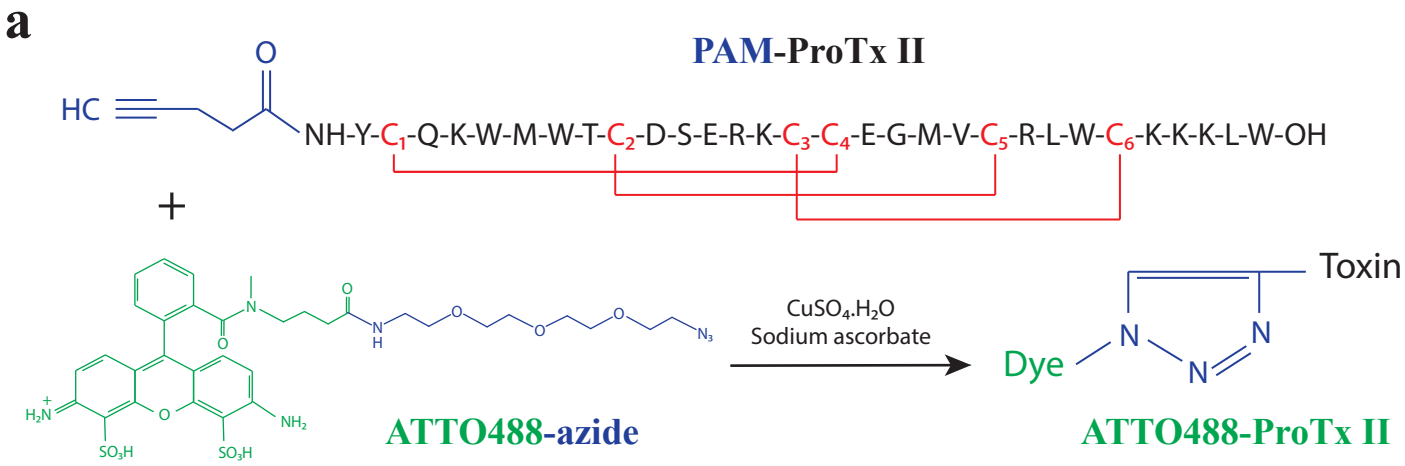
a
PAM-ProTx II
HC
NH-Y-C1-Q-K-W-M-W-T-C2-D-S-E-R-K-C3-C4-E-G-M-V-C5-R-L-W-C6-K-K-K-L-W-OH
+
CuSO4.H2O
Sodium ascorbate
Toxin
Dye
ATTO488-azide
ATTO488-ProTx II

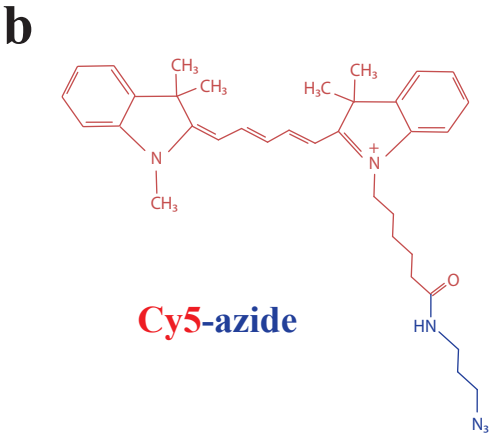
b
Cy5-azide

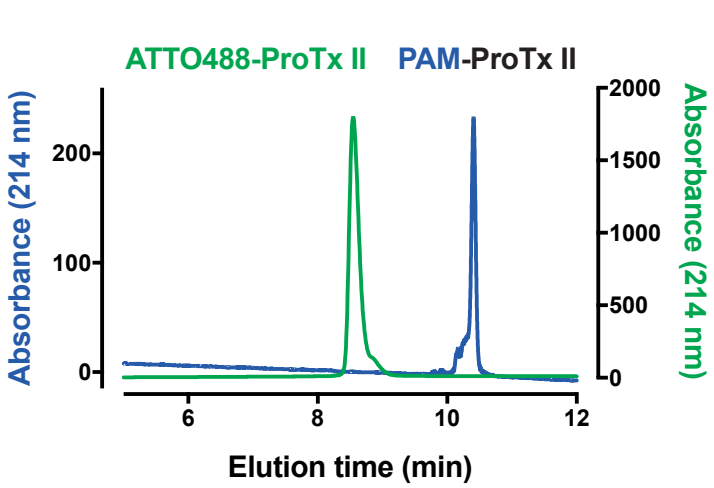
c
ATTO488-ProTx II
PAM-ProTx II
Absorbance (214 nm)
Absorbance (214 nm)
Elution time (min)

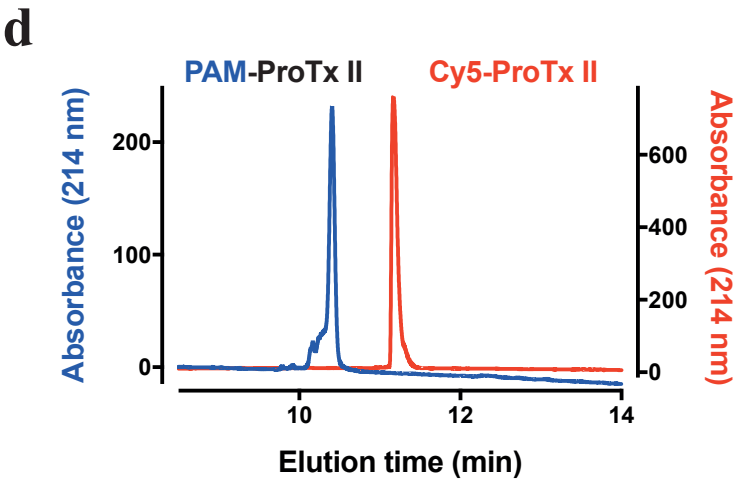
d
PAM-ProTx II
Cy5-ProTx II
Absorbance (214 nm)
Absorbance (214 nm)
Elution time (min)

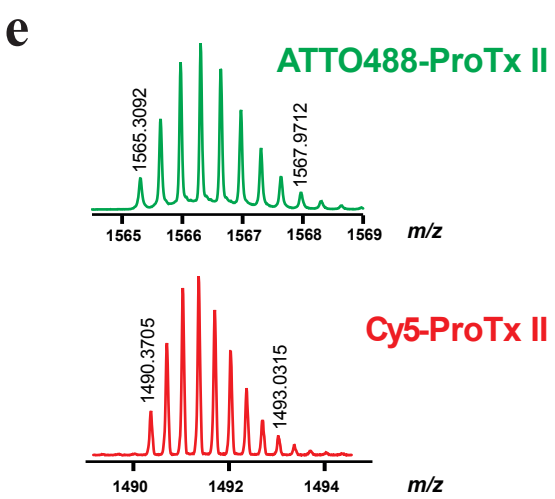
e
ATTO488-ProTx II
1565.3092
1567.9712
m/z
Cy5-ProTx II
1490.3705
1493.0315
m/z

Figure 3

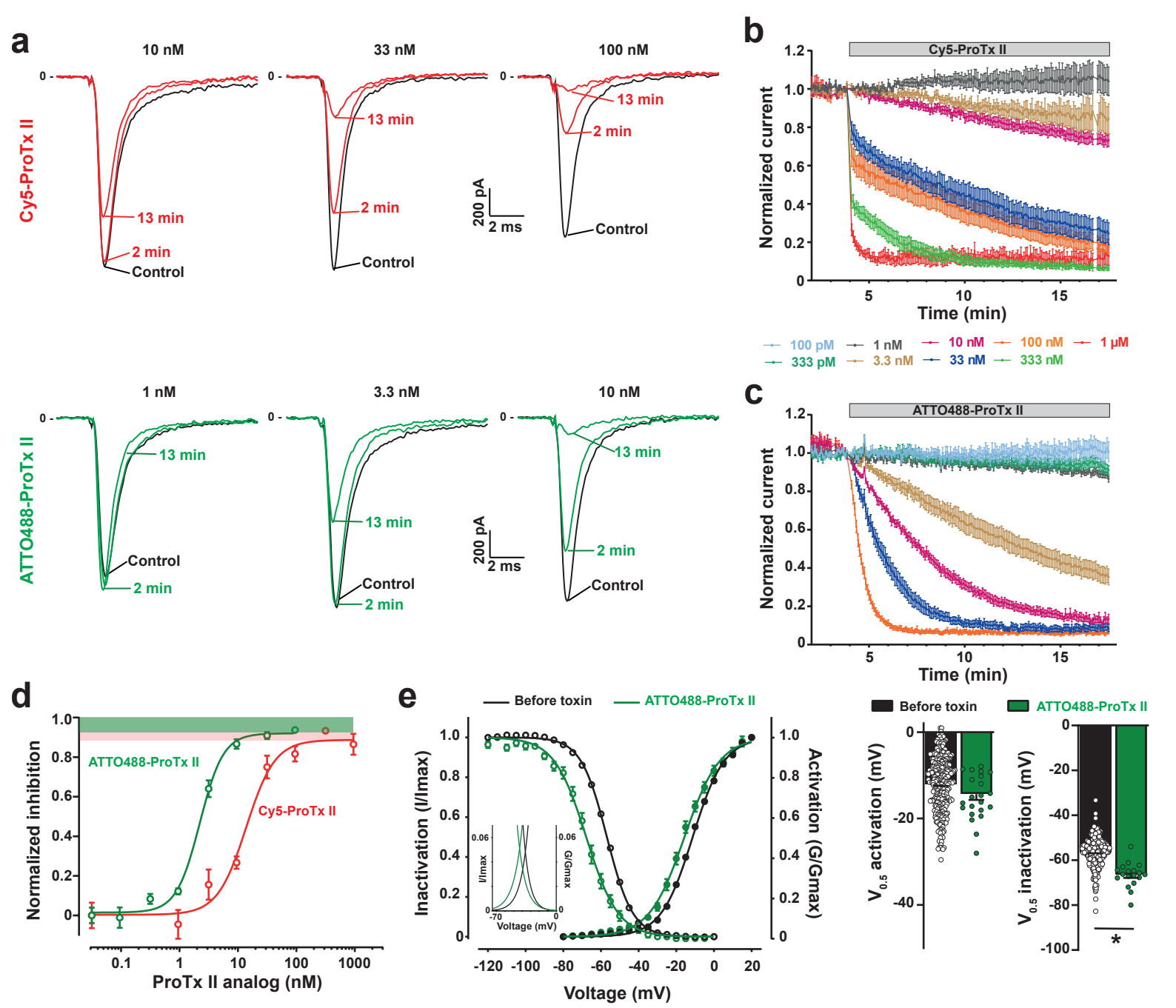
a
10 nM
33 nM
100 nM
Cy5-ProTx II
13 min
2 min
Control
200 pA
2 ms
1 nM
3.3 nM
10 nM
ATTO488-ProTx II
b
Cy5-ProTx II
Normalized current
Time (min)
100 pM
1 nM
10 nM
100 nM
1 µM
333 pM
3.3 nM
33 nM
333 nM
c
ATTO488-ProTx II

d
Normalized inhibition
ATTO488-ProTx II
Cy5-ProTx II
ProTx II analog (nM)
e
Before toxin
ATTO488-ProTx II
Inactivation (I/Imax)
Activation (G/Gmax)
Voltage (mV)
V0.5 activation (mV)
V0.5 inactivation (mV)
*

Figure 4

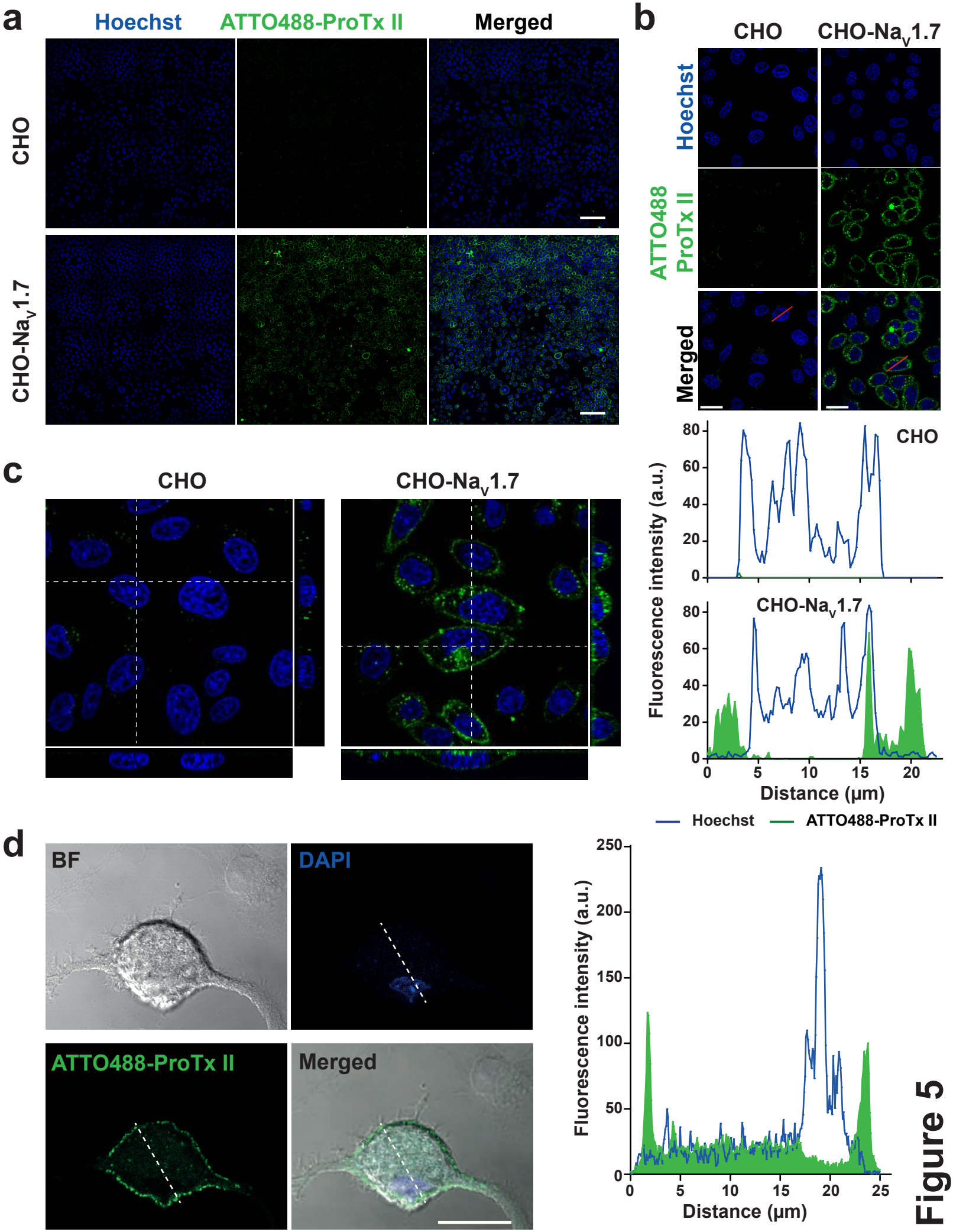
a
Hoechst
ATTO488-ProTx II
Merged
CHO
CHO-Na$_V$1.7
b
CHO
CHO-Na$_V$1.7
Hoechst
ATTO488 ProTx II
Merged
CHO
CHO-Na$_V$1.7
Fluorescence intensity (a.u.)
Distance (μm)
Hoechst
ATTO488-ProTx II
c
CHO
CHO-Na$_V$1.7
d
BF
DAPI
ATTO488-ProTx II
Merged
Fluorescence intensity (a.u.)
Distance (μm)

Figure 5

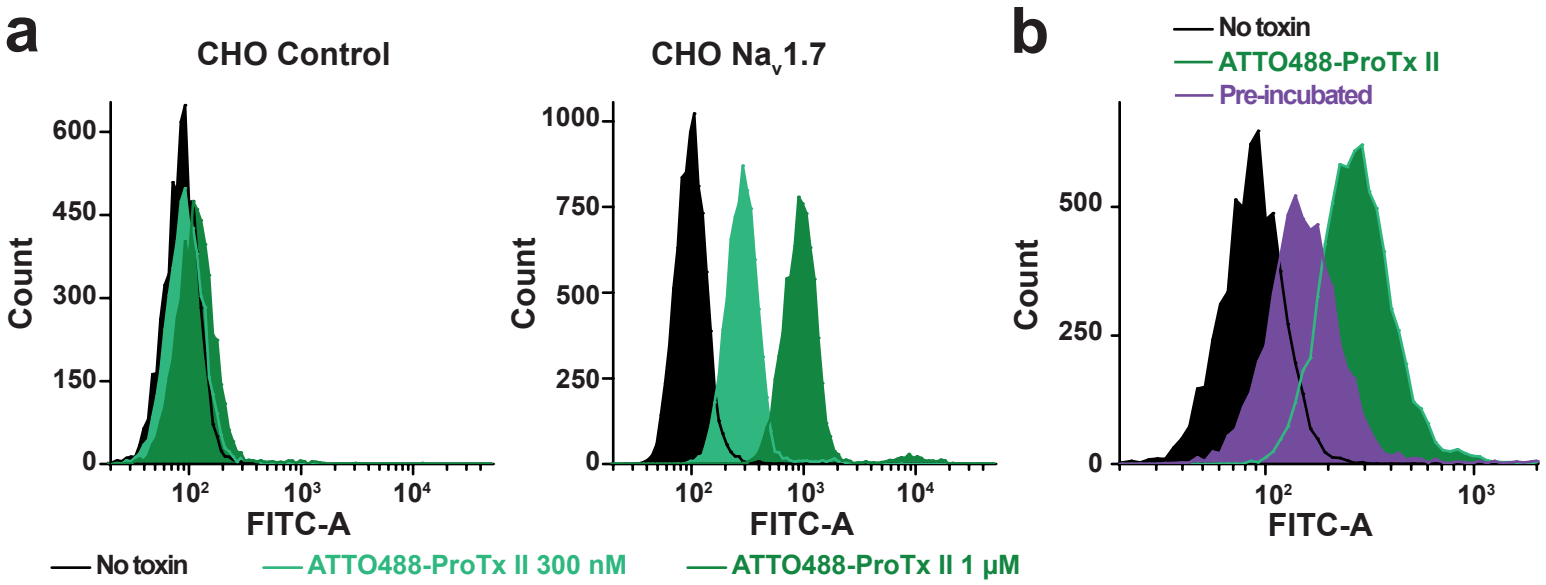
a
CHO Control
CHO Na$_v$1.7
b
No toxin
ATTO488-ProTx II
Pre-incubated
Count
FITC-A
No toxin
ATTO488-ProTx II 300 nM
ATTO488-ProTx II 1 µM

Figure 6

Table I. Inactivation kinetics of $Na_v1.7$ channels upon application of ProTx II analogues

	Fast time constant (ms)	Slow time constant (ms)	Af/As
ProTx II			
t = 0 min	0.74 ± 0.11 (n= 6)	2.35 ± 0.45 (n= 6)	15.2 ± 6.1 (n= 6)
t = 13 min	0.59 ± 0.06 (n= 6)	3.30 ± 0.79 (n= 6)	28.3 ± 7.1 (n= 6)
8His-ProTx II			
t = 0 min	1.02 ± 0.15 (n= 7)	2.17 ± 0.61 (n= 7)	6.4 ± 3.5 (n= 7)
t = 13 min	0.82 ± 0.12 (n= 7)	2.85 ± 0.69 (n= 7)	6.3 ± 2.8 (n= 7)
Biot-ProTx II			
t = 0 min	0.64 ± 0.03 (n= 6)	4.31 ± 0.62 (n= 6)	26.49 ± 3.2 (n= 6)
t = 13 min	1.16 ± 0.34 (n= 6)	3.74 ± 1.30 (n= 6)	17.7 ± 8.8 (n= 6)
ATTO488-ProTx II			
t = 0 min	1.01 ± 0.15 (n= 7)	2.28 ± 0.50 (n= 7)	9.6 ± 4.1 (n= 7)
t = 13 min	0.68 ± 0.07 (n= 7) *	3.69 ± 0.55 (n= 7)	33.2 ± 7.8 (n= 7) *
Cy5-ProTx II			
t = 0 min	0.78 ± 0.07 (n= 7)	2.97 ± 0.78 (n= 7)	18.1 ± 9.1 (n= 7)
t = 13 min	0.63 ± 0.04 (n= 7)	2.89 ± 0.49 (n= 7)	20.3 ± 5.6 (n= 7)

Paired *t*-test, * $p < 0.05$

Table II. K_{ON} (min) of inhibition of $Na_v1.7$ channels by PrTx II analogues.

	333 nM	100 nM	33 nM	10 nM	3.3 nM
ProTx II	0.45	1.17	1.34	6.57	8.61
8His-ProTx II	1.61	9.71	-	-	-
Biot-ProTx II	0.22	0.45	0.66	6.50	2.51
ATTO488-ProTx II	-	0.66	1.89	4.63	14.86
Cy5-ProTx II	2.8	12.0	9.35	43.84	24,77